TRIUMF

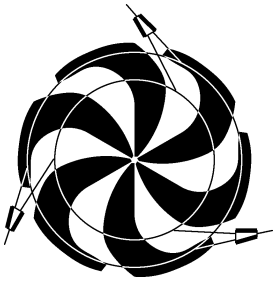

ANNUAL REPORT
SCIENTIFIC ACTIVITIES
1999

ISSN 1492-417X

CANADA'S NATIONAL LABORATORY
FOR PARTICLE AND NUCLEAR PHYSICS

OPERATED AS A JOINT VENTURE

MEMBERS:

THE UNIVERSITY OF ALBERTA
SIMON FRASER UNIVERSITY
THE UNIVERSITY OF VICTORIA
THE UNIVERSITY OF BRITISH COLUMBIA

ASSOCIATE MEMBERS:

CARLETON UNIVERSITY
THE UNIVERSITY OF MANITOBA
L'UNIVERSITÉ DE MONTRÉAL
QUEEN'S UNIVERSITY
THE UNIVERSITY OF REGINA
THE UNIVERSITY OF TORONTO

UNDER A CONTRIBUTION FROM THE
NATIONAL RESEARCH COUNCIL OF CANADA

JULY 2000

The contributions on individual experiments in this report are outlines intended to demonstrate the extent of scientific activity at TRIUMF during the past year. The outlines are not publications and often contain preliminary results not intended, or not yet ready, for publication. Material from these reports should not be reproduced or quoted without permission from the authors.

Experiment 560
Low energy $\pi^{\pm}\vec{p}$ analyzing powers with CHAOS
(G.R. Smith, TRIUMF; J. Patterson, Colorado)

This experiment made use of the CHAOS spectrometer and a specially designed CHAOS polarized proton target (CPPT). The goal was to measure the analyzing powers (A_y) for $\pi^{\pm}p$ scattering to better than ± 0.05 between angles of $\approx 60^\circ$ and 180° at several bombarding energies between 30 and 140 MeV. In 1995/1996 we made measurements at resonance energies only, due to persistent problems with the polarized target. In the fall of 1997, however, the target (and spectrometer) operated flawlessly, which permitted us to successfully explore the low energy region with incident π^- down to 51 MeV. Unfortunately, the beam time available to us in the fall of 1997 was insufficient to measure below 51 MeV, or to pursue the π^+ part of the low energy program. Since the Polarized Target Group is committed to ISAC experiments for the foreseeable future, data acquisition for Expt. 560 is finished.

Using the technique of single energy partial wave analysis (PWA), the data obtained in this experiment will be used to filter out differential cross section ($\frac{d\sigma}{d\Omega}$) measurements which are inconsistent with the A_y data. At present the low energy $\frac{d\sigma}{d\Omega}$ database contains a number of gross inconsistencies between experiments. In order to determine the πN PW amplitudes with precision, reliable and precise $\frac{d\sigma}{d\Omega}$ data (which fix the larger amplitudes) must be combined with reliable and precise A_y data (which fix the smaller amplitudes). Analyzing power results in the forward angle (Coulomb-nuclear interference) region for π^+p scattering, and in the S–P interference region at backward angles near 50 MeV for π^-p scattering are especially useful in this regard. With accurate πN partial waves, in particular at low energies, the physics goals of Expt. 560 are then to provide improved values for the πN coupling constant, to extrapolate to threshold where the πN scattering lengths can be obtained, and to extrapolate below threshold as well as to obtain a more accurate measure of the πN sigma term. The πN sigma term is an explicit measure of chiral symmetry breaking from which the strange sea quark content of the proton can be deduced.

In 1997 the analysis of the resonance energy experiment was completed, and a Ph.D. thesis [Hofman] was obtained based on those data. In 1998 the resonance energy results were published [Hofman *et al.*, Phys. Rev **C58**, 3484 (1998)]. In this year's progress report, we focus on the analysis of the low energy π^-p data obtained in the fall, 1997, Expt. 560 running period.

As a result of the many previous problems with the CPPT, the experiment took place in the M11 channel rather than the (low energy) M13 channel. In M11 the target polarization could be checked by comparison to previous measurements of A_y at resonance energies. This check was performed at the start of the measurement (140 MeV incident π^+) and verified the target polarization determined by NMR techniques was indeed ≈ 0.80.

Due to the fact that data were acquired with CHAOS at $\pm\theta$ simultaneously, the only other quantity that had to be measured was the πp scattering yield. Measurements of other factors, such as the relative flux of incident pions, etc., were unnecessary due to the self-normalizing features of analyzing power measurements with CHAOS. Another crucial feature was that the complete angular distributions were measured simultaneously. The experiment would not have been practical otherwise, due to the extremely low cross sections involved and subsequent long running times associated with standard angle-by-angle measurements.

As a result, in what turned out to be a very successful run, data were acquired for incident π^- at 51, 57, 67, 87, 98, 117, and 139 MeV. Graphite background data were also collected. The resulting database spans the S–P interference region which is 'centred' at 57 MeV, 180°. Most of the beam time was devoted to the 57 MeV measurement. There the backward angle cross sections are less than 1 μb/sr, more than 3 orders of magnitude less than the corresponding cross sections at 140 MeV. However, it has been shown that the greatest sensitivity to the scattering lengths is right at the S–P interference minimum, so enough time was spent collecting data in this most difficult region to obtain approximately ± 0.08 uncertainty at the most backward angle, with uncertainties at most other angles (and energies) typically ± 0.02 or less.

In order to obtain data at the smallest possible θ at the lowest three energies in particular, the CHAOS first level trigger (1LT) was programmed for 'singles' mode so that any scattered pion could generate a 1LT. This would have led to an overwhelming background of quasi-elastic π^-n scattering (the polarized target consists of butanol, C_4H_9OH) were it not for the innovative changes which were made to the second level trigger (2LT). The 2LT was programmed to recognize 'short tracks', i.e. protons which were observed in the correct angular region and with the expected curvature based exclusively on information from only the inner two wire chambers WC1 and WC2. Events with (recoil) protons whose trajectories stopped outside of WC2 were not lost; if the protons failed to make it out to WC3, their trajectories were determined by combin-

ing the pion vertex with the hits registered in WC1/2. Events with proton tracks out at least to WC2 were required in the 2LT, which reduced overall trigger rates to manageable levels (typical live times were ≈90–95%) without having to resort to a doubles 1LT, which would have considerably abbreviated the measured angular distributions at the lowest energies.

Over the last two years much effort was expended in designing and implementing an analysis procedure for the data which emphasized increased efficiency. The linear data streams were converted into a tree structure to provide increased performance of data access and retrieval. Software was built around the CERN ROOT system, and thus adopted its object oriented philosophy. This led to an extremely fast, robust, and automated analysis that lets us adjust parameters such as kinematic cuts and angular binning, checking the new results in seconds rather than days.

The analysis is nearing completion. The only significant hurdles left are to properly subtract the (measured) background from the angular yields, and to recognize backscattering events. Both of these hurdles are only significant at energies of 67 MeV and lower. Algorithms are under development which aim to recognize pions backscattering from WC2 or WC3 downstream of the target. A small subset of this class of events passed our trigger requirements, since the track segment of the backscattered π^- which heads backwards towards the target looked like a short track proton and was accepted if the backscattered trajectory passed through the target region. The remainder of the backscattered track then had the appearance of a scattered π^-. These events clearly have singular characteristics, and several methods of dealing with them appear to be effective.

Results between 139 MeV and 87 MeV are shown in Fig. 32 and Fig. 33. Due to the background issues mentioned above, the results below 67 MeV are still being worked on, while the higher energies are fairly final. The agreement with the prediction of the phase shift solution SM95 is good at the energies analyzed so far.

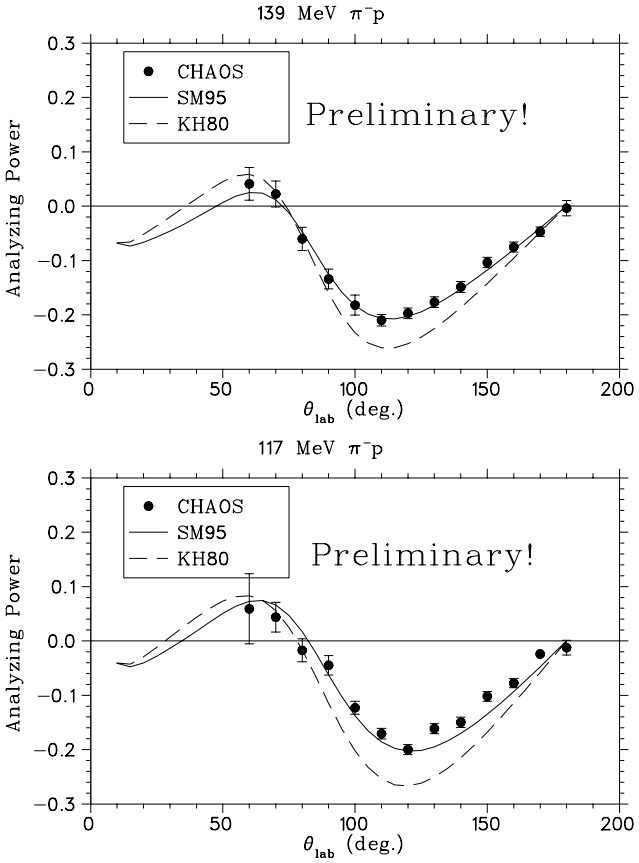

Fig. 32. Preliminary results for the $\pi^- p$ elastic scattering analyzing power measured with CHAOS at 139 MeV (upper) and 117 MeV (lower) are compared with the predictions of the phase shift analysis SM95 (solid curves) and KH80 (dashed curves).

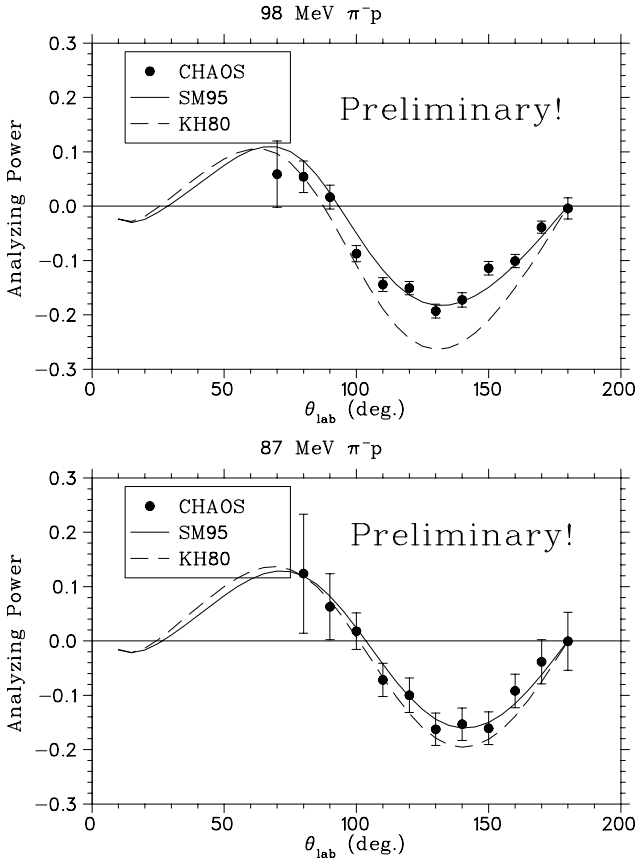

Fig. 33. Preliminary results for the $\pi^- p$ elastic scattering analyzing power measured with CHAOS at 98 MeV (upper) and 87 MeV (lower) are compared with the predictions of the phase shift analysis SM95 (solid curves) and KH80 (dashed curves).

Experiment 561
Determination of the $\pi^{\pm}p \rightarrow \pi^{\pm}\pi^{+}n$ cross section near threshold
(M. Sevior, Melbourne)

The aim of Expt. 561 was to measure the total cross sections for the reactions $\pi^+p \rightarrow \pi^+\pi^+n$ and $\pi^-p \rightarrow \pi^-\pi^+n$ as close to threshold as possible. At these very low energies it is possible to use heavy baryon chiral perturbation theory to relate the total cross sections to the isospin 0 and isospin 2 scattering lengths which are fundamental parameters of low energy QCD. The final paper from this experiment was accepted by Physical Review C for publication in 2000.

Our final results for the $\pi^+p \rightarrow \pi^+\pi^+n$ reaction are:

Table III. $\pi^+p \rightarrow \pi^+\pi^+n$ cross sections.

$T_{\rm beam}$	Cross section (μb)		
(MeV)	one-pion	two-pion	average
200 ± 1	1.4 ± 0.4	1.4 ± 0.3	1.4 ± 0.3
184 ± 1	0.30 ± 0.07	0.30 ± 0.07	0.30 ± 0.07

For the $\pi^-p \rightarrow \pi^-\pi^+n$ reaction our results are:

Table IV. Cross sections for the π^- channel of the reaction.

$T_{\rm beam}$ (MeV)	Cross section (μb)
200	6.54 ± 0.91
190	2.99 ± 0.48
184	1.85 ± 0.27
180	0.74 ± 0.11
176	0.18 ± 0.14

Applying the heavy baryon chiral perturbation theory calculations of Bernard, Kaiser and Meissner to our results leads to the following values of the $\pi - \pi$ scattering lengths. Here our results are compared to chiral perturbation theory predictions with varying assumptions.

Table V. Comparison of theoretical and experimental values for the $\pi - \pi$ scattering lengths. The uncertainties include both statistical and systematic errors.

Reference	$a_0[m_\pi^{-1}]$	$a_2[m_\pi^{-1}]$
Gasser & Leutwyler	0.20 ±0.01	-0.042 ±0.002
Bijnens *et al.*	0.2156	-0.0409
Girlanda *et al.*	0.209 ± 0.004	-0.045 ± 0.006
This experiment	0.23 ± 0.08	-0.031 ± 0.008

The error in the experimental results quoted is dominated by the theoretical uncertainty in relating the cross sections to scattering lengths. We regard this as a challenge for our Theoretical colleagues. Improving the uncertainty for the isospin 2 appears both tractable and worthwhile. The calculations converge quickly for the isospin 2 channel. In addition there appear to be no other prospects for experimental investigation for this isospin combination. The new K_{e4} experiments at Brookhaven and DAΦNE and the pionium experiment at CERN are sensitive to the isospin 0 scattering length.

Experiment 700
Measuring cross sections of long-lived radionuclides produced by 200–500 MeV protons on elements found in lunar rocks and meteorites
(J. Sisterson, Massachusetts General Hospital & Harvard Medical School)

Targets were irradiated in 1993, 1996 and 1997 at 200, 300, 400 and 500 MeV at TRIUMF. These measurements are part of a systematic study to measure both proton and neutron production cross sections needed to understand the interactions of cosmic rays with extraterrestrial materials. Small quantities of radionuclides and stable isotopes are produced in lunar rocks and meteorites in these interactions. If we can interpret these cosmogenic nuclide archives we can learn the history of the object or of the cosmic rays. The models used in these analyses require good knowledge of all relevant production cross sections.

Analysis continues on the targets irradiated at TRIUMF; it may take several years before these measurements are completed. Long-lived radionuclides produced in the targets are measured using accelerator mass spectrometry, stable isotopes using mass spectroscopy and relatively short half-life radionuclides (half-lives less than ∼5 years) by non-destructive gamma-ray spectroscopy.

In Table VI, we present new cross section measurements for the reaction $\mathrm{Ti}(p,x)^{14}\mathrm{C}$. These values were presented at the 30th Lunar and Planetary Science Meeting held in Houston, Texas, in March [Sisterson *et al.*, in Lunar and Planetary Science XXX, Abstract #1202 (Lunar and Planetary Inst., Houston, 1999)]. These cross section measurements were completed after ^{14}C proton production cross sections from oxygen, magnesium, silicon, iron and nickel were published [Jull *et al.*, Geochim. Cosmochim. Acta **62**, 3025 (1998)].

Table VI. $\mathrm{Ti}(p,x)^{14}\mathrm{C}$ cross section measurements.

Energy	Cross section
MeV	mb
100 ± 3.0	0.010 ± 0.001
200	0.037 ± 0.002
300	0.073 ± 0.004
400	0.152 ± 0.008
500	0.217 ± 0.011

New proton production cross sections for the cross sections Fe$(p,x)^{52}$Mn, Fe$(p,x)^{54}$Mn, Ni$(p,x)^{52}$Mn and Ni$(p,x)^{54}$Mn measured in irradiations made at TRIUMF in 1993 will be reported at the 31st Lunar and Planetary Science Meeting to be held in Houston, Texas, March, 2000 [Sisterson *et al.*, in Lunar and Planetary Science XXXI, Abstract #1432, (Lunar and Planetary Inst., Houston, in press)].

Experiment 704
Charge symmetry breaking in $np \to d\pi^0$ close to threshold

(A.K. Opper, Ohio; E. Korkmaz, UNBC)

Experiment 704 continues to make significant progress towards a high precision measurement of charge symmetry breaking in the strong interaction. The observable of interest is the forward-backward asymmetry (A_{fb}) in $np \to d\pi^0$, which must be zero in the centre-of-mass if charge symmetry is conserved and has a predicted value of -35×10^{-4} [Niskanen, Few Body Syst. **26**, 241 (1999)]. The experiment was carried out with a 279.5 MeV neutron beam, a liquid hydrogen target, and the SASP spectrometer positioned at 0°. With these kinematics and the large acceptance of SASP, the full deuteron distribution was detected in one setting of the spectrometer thereby eliminating many systematic uncertainties. A measurement of the $pp \to d\pi^+$ distribution accompanied the primary measurement as a robust test of the analysis and simulation codes, since the deuteron distribution from $pp \to d\pi^+$ must be symmetric in the centre of mass due to the indistinguishability of the two protons.

Almost 1/3 of all the data were acquired in a period of essentially continuous running from mid-April to mid-August. With the completion of production data acquisition, new resources have become available to thoroughly examine the simulation. In this process the basic GEANT packages have been tested for suitability with Expt. 704 and a number of inconsistencies removed. Work then successfully progressed on the description of the background in the $np \to d\pi^0$ data and is now focusing on the shape of the $np \to d\pi^0$ deuteron locus. Simulations of some of the auxiliary measurements (e.g. np elastic scattering, H^0 running, and p-beam measurements) have been fruitful in that they have provided valuable information on the possibility of a low energy tail in the primary proton beam and are highly sensitive to the SASP acceptance. These comparisons of data with simulation have led to investigating the model used to describe the SASP magnetic fields. There are many areas currently under investigation and we now have the tools and human resources to see this measurement to completion.

Data acquisition

At the beginning of the summer running period Expt. 704 had approximately 5.2 million $np \to d\pi^0$ events and 6.5 million $pp \to d\pi^+$ events on tape. The summer running period has raised these numbers to 6.9 million and 9.4 million, respectively. This will produce a statistical uncertainty of 9.4×10^{-4}; as many of the systematic effects are themselves determined by statistics, these data should yield a systematic uncertainty of 12×10^{-4}.

A standard cycle of data-taking includes acquisition of $np \to d\pi^0$ and $pp \to d\pi^+$ with the target full and empty, as well as np elastic, H^0 and p-beam data to determine the energy distribution and origin of the incident beam and the relative position of the wire chambers to the SASP magnets. A number of additional calibration measurements were carried out this summer as this run period was intended to be the final acquisition period for Expt. 704.

Data analysis

Expt. 704 production data are analyzed in four successive passes: (1) detector calibration; (2) beam direction determination in the SASP-centric FEC coordinate system; (3) "final" extraction of the deuteron kinematic locus; and (4) efficiency determination. Analysis of all $np \to d\pi^0$ data has been completed and the $pp \to d\pi^+$ data analysis should be done by the end of January, 2000. Additional time has been needed to develop and implement code to reduce charged particle background that exists for the $pp \to d\pi^+$ data but not for the $np \to d\pi^0$ data. Application of these codes required a complete reanalysis of the $pp \to d\pi^+$ data taken prior to summer, 1999. As of this date all $pp \to d\pi^+$ data have passed through the second stage of analysis (with the new code) and the third pass has just begun. Analysis of the auxiliary measurements that were made this summer has yielded information on relative target thickness, backgrounds, and scintillator detection efficiency.

Proton background in $pp \to d\pi^+$

The method employed to study proton backgrounds in the FECs involves defining an "accidentals" time cut on the wire plane TDC values reported by the hit-decoding subroutine. The accidentals TDC window has the same width as the standard ("trues") window used for deuteron hit decoding (2.5 beam bursts), but is shifted in time with respect to the trues window to exclude the deuteron region. The FEC hits decoded in this accidental TDC time region are thus expected to be generated predominantly by background beam protons. Analysis of $pp \to d\pi^+$ data taken from 7/97 to 7/98 indicates that the number of FEC accidentals

tracks reconstructed in this fashion is approximately 30% of the number reconstructed in the trues region, with variations of 3% over the series of data cycles in this period. This does not imply, however, that one third of all deuteron *tracks* decoded from the FEC information in the trues timing window are accompanied by a secondary proton *track*. The actual proton track contamination will be an order of magnitude smaller due to (1) the efficiency for proton detection in each FEC plane is on the order of 70%, and (2) the FEC tracking algorithm requires 'second' tracks to have a hit in each of the six planes.

In summary, these preliminary investigations of FEC proton backgrounds indicate that an understanding of the efficiency of particle detection in the FEC planes constitutes an essential element in the full simulation's model of the effect of this background on the tracking. The efficiency for detection of pions must be similarly incorporated. Extraction of this detection efficiency from data taken with the Expt. 704 triggers is currently under way.

Similar analysis of TDC data from the VDCs (in the SASP focal plane) can be combined with that from the FECs to investigate the low-energy proton tail component of the background in the standard locus spectrum. From this analysis it is clear that track matches involving focal plane proton tail tracks contribute on the order of 10% of the counts in the standard locus spectrum for reaction angles below 10 mr. This estimate of the tail-rate fraction typically varies from 13% to 15% over the data cycles from 7/97 to 7/98. The shapes and overall intensities of the VDC accidentals spectra serve as benchmarks for the full simulation's reproduction of the proton tail-related background.

The particle identification cut which is based on energy deposition in the "B" paddles and the time of flight through the SASP (LTOF) reduces most of these accidental protons. A technique employing the relative time between the event and the cyclotron rf (LTRF) has been developed to further reduce this background by 30%.

GEANT simulation of Expt. 704

Recent developments of the Expt. 704 GEANT simulation have focused on the following issues: (1) reproducing the shape of the $np \rightarrow d\pi^0$ background; and (2) testing the model of the SASP magnetic field.

Modelling of (n, d) background

Target empty $np \rightarrow d\pi^0$ data provide a useful guide to the shape of the deuteron backgrounds arising from (n, d) reactions on non-hydrogen materials. A straightforward background subtraction of target empty from target full is not possible due to differing energy losses and multiple scattering suffered by background deuterons. A technique investigated in fall, 1999 treats the background in the locus histogram as a smooth surface to be modelled by a functional form in the (reaction angle, momentum) plane. Thus in this scheme no attempt is made to reproduce the background from a "realistic" model of (n, d) scattering events in the front-end. Rather, the observable portions of the background in the "locus-free" regions of the (angle, momentum) histogram provide the only constraints on the model of the background beneath the locus.

A fit to the sum of 8/97 through 5/99 target empty data using a single GEANT background-free locus (with hydrogen interaction sites in the front-end scintillators and LH_2 target walls) and an analytic background function produced a χ^2/d.f. of 1.5 (see Fig. 34). The shape of the background was judged to be reproduced accurately enough with this fitting method that further work on the target full data (discussed below) could focus primarily on the hydrogen locus model.

Modelling of $np \rightarrow d\pi^0$ target full data

The sum of 8/97 through 5/99 target full locus data over the nominal "full acceptance" target variable region of 16 cm^2 [(–2,2) cm in the vertical position, XI, by (–2,2) cm in the horizontal position, YI] was fit using a sum of a single GEANT background-free locus and the same 8-term background functional form described above. The fit yielded a χ^2/d.f. of 4.4 (see Fig. 35). The increase in χ^2 from the target empty fit is due to much greater statistical sensitivity to the locus signal; thus the locus is relatively poorly described in comparison to the smooth background. Features of the full-acceptance fit include the following:

- The "shelf" of background at the low- and high-momentum ends of the momentum-projected locus spectrum is well reproduced. This gives some confidence that the background shape is sufficiently well described.
- The positions of the locus "lobes" of the momentum-projected spectrum for reaction angles less than 10 mr are well reproduced by the simulation. The centroid of the distribution in reaction angle (i.e. the "turnaround angle" of the locus) is also well reproduced. The yield near the turnaround is overpredicted by the model.
- The overall width of the momentum-projected locus spectrum is fairly well reproduced.
- The simulation underpredicts the strength in the high-momentum end of the locus.

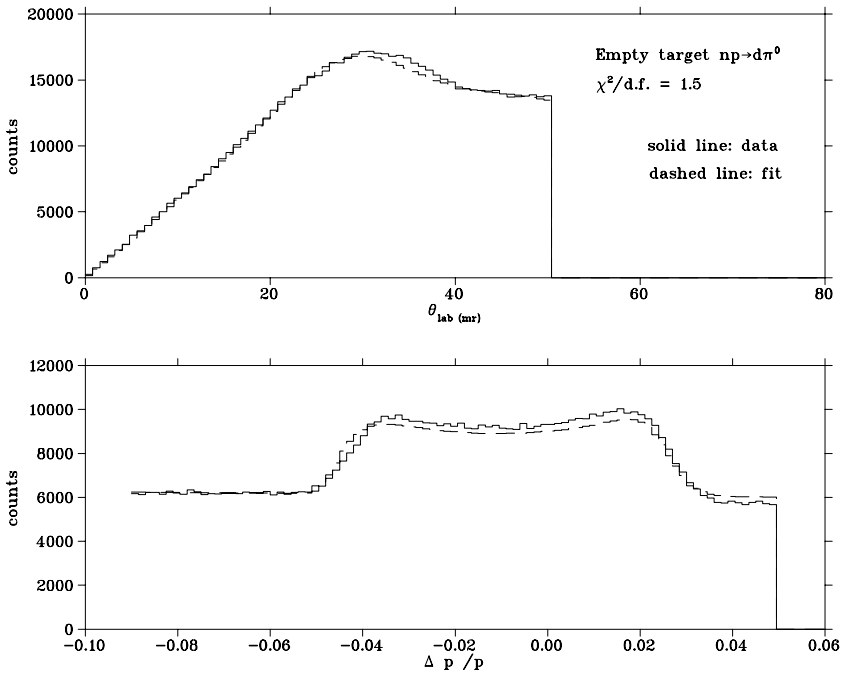

Fig. 34. GEANT fit to sum of 10/97 through 5/99 empty target $np \rightarrow d\pi^0$ data, full (XI,YI) acceptance. Upper panel is the locus projection on the reaction angle axis for relative momenta in the range –9% to 5%. Lower panel is the projection on the momentum axis for reaction angles in the range 0 to 50 mr.

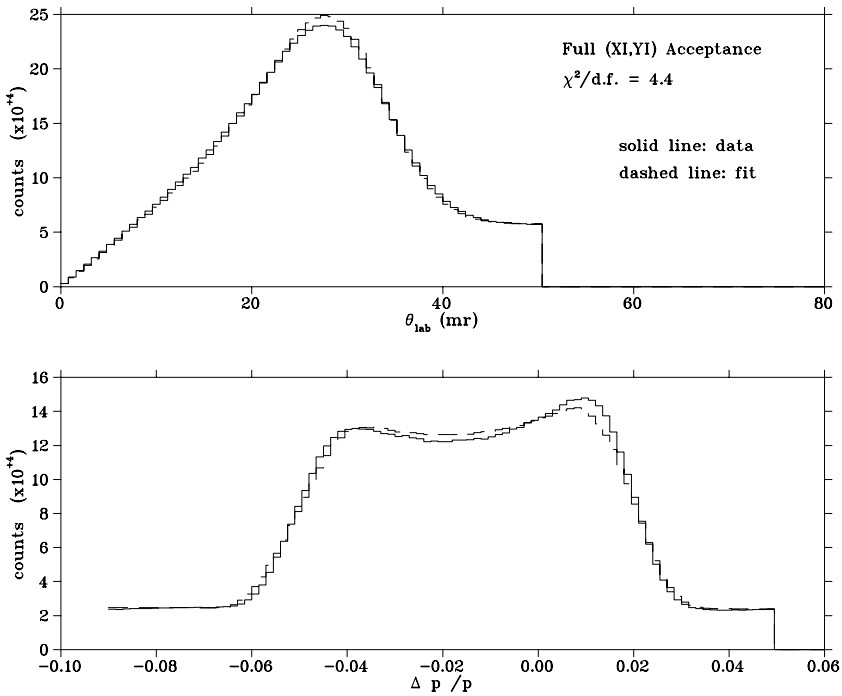

Fig. 35. GEANT fit to sum of 8/97 through 5/99 full target $np \rightarrow d\pi^0$ data, full (XI,YI) acceptance. Panels are described in the caption of Fig. 34.

The fact that the simulation does not reproduce either the gross yields or the instrumental asymmetry observed in the data is presumably evidence that the SASP angular acceptance, and the momentum variation of this acceptance, is not yet correctly described. Investigations of the SASP acceptance model via simulation of np elastic data are in progress.

Simulation of the H^0 and np elastic data

Progress has also been made with regard to the GEANT simulation of the auxiliary H^0 beam and np

elastic data taken in each cycle along with $np \to d\pi^0$. One important goal of these studies is to obtain an independent determination of the energy profile of the primary proton beam impinging on the ^{7}Li target. This has been achieved by allowing parameters representing the centroid and width of the proton beam as well as a possible low-energy tail to vary until the observed H^0 momentum distribution at the focal plane was correctly reproduced by GEANT. The results indicate that the primary beam has a negligible low-energy tail and is typically best represented by a Gaussian with a FWHM of 0.47 MeV. Comparisons between data and simulation for the np elastic case provided consistency with the beam properties as deduced from the H^0 studies. That is, the same primary proton beam parameters simultaneously produce the observed average locations and widths of the H^0 and np elastic proton peaks at the focal plane.

The np elastic data in addition allow for a thorough investigation of how well GEANT is reproducing the optical properties of SASP for momentum rays originating from within the full acceptance volume (vertical and horizontal positions and angles) used in the $np \to d\pi^0$ analysis. Investigation of the dependence of the focal plane proton peak centroids and widths on the position or scattering angle at the target reveal good agreement between data and simulation if analysis is restricted to a small acceptance volume. However, some discrepancies do exist if the full acceptance employed in the analysis is used. These discrepancies, which could result from a mismatch in one or two of the SASP optical parameters, are currently being investigated.

Optics simulation for Expt. 704

The SASP dipole has a non-uniform gap, and Expt. 704 takes data with the spectrometer powered up to a higher magnetic field than was ever measured in the comprehensive field maps of the SASP dipole. Magnetic saturation causes the dipole magnetic field to sag in the high-field (small gap) region, relative to the ideal.

Measurements of the SASP magnetic field at the Expt. 704 settings exist only along one line in the interior field region of the SASP dipole. We parameterize the ratio R

$$R = B(\text{measured})/B(\text{ideal})$$

as a function of the gap in the dipole. We then assume that this deficiency function R is applicable over the whole of the SASP dipole.

As a test of how well the magnetic fields of the spectrometer are modelled, we can compare calculations with two sets of experimental data, namely (1) the measurements of the SASP dispersion, taken with high resolution $^{208}\text{Pb}(p,p')$ (small beamspot on target), and (2) measurements of (n,p) elastic scattering (large secondary beam on target).

This model of the SASP dipole is able to reproduce the dispersion calibration data to good accuracy, except that the calculated ray positions systematically deviate from the measured positions by about 1 cm. (By contrast, using the dipole fields with no saturation yields a discrepancy between raytracing and measured positions of about 10 cm.) The present model gives a good account of dispersion found for the np elastic measurements, but cannot yet account for a small $(x/x\theta)$ optical aberration observed in the data.

It is known that magnetic saturation not only changes the shape of the field, as modelled by the deficiency function R, but also changes the effective edge angles of the dipole, as well as causing the effective field boundaries to move out away from the dipole (i.e. giving more field for the particles to bend in). We are presently incorporating these features in our model of the dipole field, and studying their effects on the optical aberrations.

Input from other mechanisms

Deuteron reactions, which amount to 1–2% losses in detector materials and are significantly momentum dependent over the 8% momentum range of the experiment, must be determined and included in the simulation. Data on total reaction cross sections of deuterons on various nuclei, of elastic scattering of deuterons by ^{1}H, ^{12}C and ^{16}O, as well as a model (due to Glauber) for deuteron breakup cross sections have been incorporated into lookup tables to be used in the GEANT simulation.

Other activities

All the data from the different phases of Expt. 704 production running ($np \to d\pi^0$ and $pp \to d\pi^+$, for both target full and empty) total approximately 24 million events. Comparable numbers of events must be simulated, scans over at least a $3 \times 3 \times 3$ parameter space (beam energy, central momentum of SASP and A_1/A_0) produced, and finally a least squares minimization carried out to extract A_{fb}. In the end, we will have simulated over 650 million events. Using only the cpu's that are currently at the disposal of Expt. 704 will require over one year to generate a sufficient number of events. To remedy this situation, Expt. 704 has applied for and been granted "Friendly User" status at the Ohio Supercomputer Center in Columbus. This will give Expt. 704 access to the OSC super-cluster of 32 quad-Pentia boxes, which will be networked and will run the same operating system currently in use by Expt. 704, Linux.

This will reduce the cpu time for Expt. 704 to less than two weeks.

Expt. 704 uses the FORTRAN based version of GEANT, GEANT3. TRIUMF is part of the effort to produce GEANT4, a C++ version that is intended to run more efficiently. Given the large amount of simulation required by Expt. 704 and the potential to reduce the cpu time, a comparison of GEANT3 and GEANT4 with the Expt. 704 specific code was carried out. The description of the front end equipment and the particle generator were converted to GEANT4 format for this investigation. A similar (stripped down) version of the standard Expt. 704 simulation was made that generated a pencil beam of 283.0 MeV deuterons 100 cm upstream of the target and the deuteron tracked through the materials and detectors at the front end. The results of the two simulations were consistent with each other and GEANT4 was approximately 9% faster than GEANT3. While a decrease in simulation time would benefit Expt. 704, the observed decrease was deemed insufficient compared to the time required to convert the whole simulation to GEANT4 format.

Experiment 715
Weak interaction symmetries in β^+ decay of optically trapped ^{37,38m}K

(J.A. Behr, TRIUMF; K.P. Jackson, TRIUMF/SFU)

TRINAT (TRIUMF Neutral Atom Trap) is close to having a preliminary number in its first experiment, the β^+-ν correlation coefficient a_F in the superallowed Fermi decay of ^{38m}K. After making technical improvements, we took a data set at ISAC in April of β^+-recoil coincidences with similar statistics to that taken at TISOL in the previous year. Analysis is in progress. If systematic errors prove to be small enough to use all of the data set, the ISAC data set will produce a measurement of the β^+-ν correlation coefficient a_F with statistical error $\approx$0.005.

To test apparatus and show the feasibility of certain future experiments, ^{80}Rb and ^{78}Rb were trapped in large quantities, and an attempt was made to trap $t_{1/2}$ = 60 ms ^{74}Rb.

The status of the off-line magneto-optical trap development for polarizing ^{41}K in preparation for ^{37}K spin correlation measurements is also summarized below.

Search for scalar currents with β-ν correlation in ^{38m}K

For β-decay studies, the magneto-optical trap (MOT) provides a sample of atoms in a localized volume with virtually zero source thickness, so unperturbed nuclear recoils can be detected in coincidence with the β, allowing the determination of the ν momentum. In the $0^+ \rightarrow 0^+$ Fermi decay of ^{38m}K, the angular distribution is given by $W[\theta] = 1 + a_F \frac{v}{c}\cos\theta$, with a_F = 1 in the standard model and a_F = –1 for a hypothetical scalar boson exchange. We measure back-to-back coincidences between β^+ and ^{38}Ar neutral atom recoils. In addition, we collect charged Ar recoils with high efficiency with a uniform electric field, and implicitly reconstruct their angular distribution; for a given E_{β^+}, $\cos(\theta_{\beta\nu})$ decreases monotonically with increasing recoil TOF.

Limits on the scalar interaction are poor, both from β decay [Adelberger, Phys. Rev. Lett. **70**, 2856 (1993); Erratum, Phys. Rev. Lett. **71**, 469 (1993)] and from particle physics. For example, direct limits on the couplings and masses of the charged Higgs were (as of 1995) such that a charged Higgs could in principle have a contribution to β decay as large as the standard model weak interaction [Herzceg, in *Precision Tests of the Standard Model*, ed. P. Langacker (1995)]. Garcia and Adelberger have now published their work at ISOLDE in the β^+-delayed proton emission of ^{32}Ar, with the result $\tilde{a}_F = a_F/(1 + b_F < \frac{m}{p} >) = 0.9989 \pm 0.0052$ (stat.) $\pm$ 0.0039 (syst.) [Adelberger *et al.*, Phys. Rev. Lett. **83** 1299 (1999); op. cit. E3101]. Fermilab D0 lower limits on scalar leptoquark masses have now reached 225 GeV [Abbott *et al.*, Phys. Rev. Lett. **80** 2051 (1998)], approximately the limit attainable from a measurement of a_F to precision 0.01 (with complementary model dependence in each case).

Present results

A plan view of the apparatus, with the small differences in detection geometry used at ISAC, is shown in Fig. 36. The recoil time-of-flight spectra for all E_{β^+}>1.1 MeV are shown in Fig. 37 for the two versions of the detector geometry used at TISOL and ISAC. The top graph shows events in the original geometry at TOF $\approx$ 1000–1200 which were kinematically forbidden, and constituted $\sim$1% of the total. They were clearly separated from the Ar^{+1} and Ar^0 events of interest, and came from atoms resting on an Al foil that fixed an equipotential at the β^+ side of the electrode assembly. Ar^{+2} recoils from this Al foil coincided with Ar^{+1}

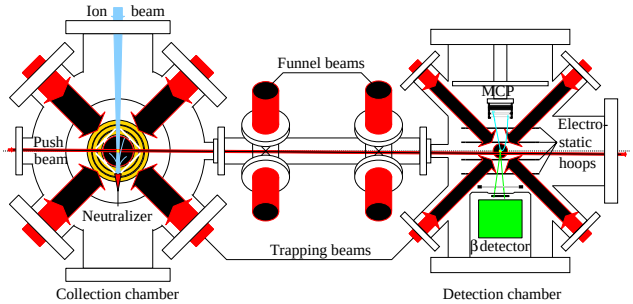

Fig. 36. Plan view of the present two-MOT apparatus.

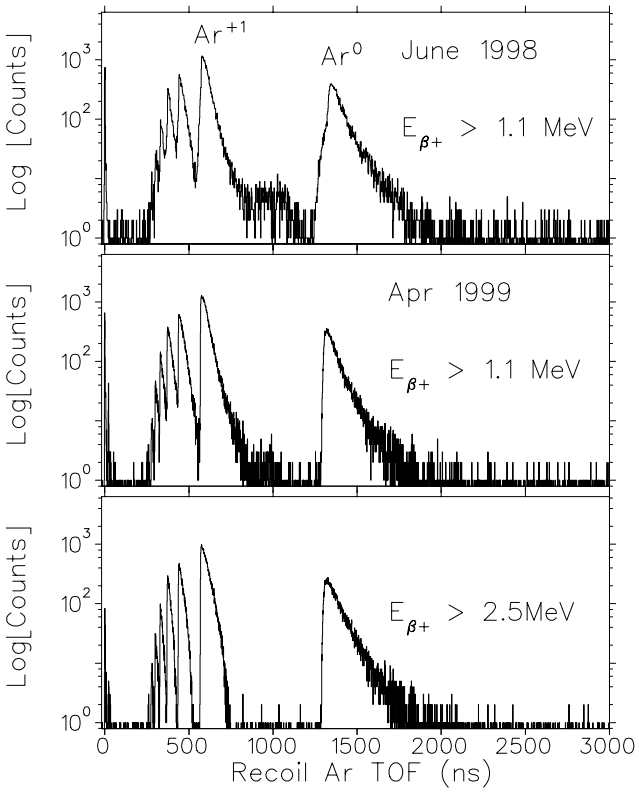

Fig. 37. TOF of Ar recoils from ^{38m}K decay, for the TISOL and ISAC data sets. Ar charge states are separated by the 800V/cm field. See text.

from the trap. The middle graph shows data taken after removing the Al foil and meshes from the apparatus, minimizing this background. The cleaner spectrum reveals backscattered betas from the MCP, making long time-of-flight ions; we can adequately model this background. The bottom graph is the TOF spectrum for $E_{\beta+}$>2.5 MeV, which has negligible background consistent with accidental coincidences.

Other improvements include a Be foil replacing the stainless steel foil separating the vacuum systems of the trap and plastic scintillator, along with an improved β^+ telescope mount placing it 1 mm from the Be foil, to minimize the effect of angle straggling on the angular resolution.

The lineshape response of the β^+ detector is a large potential systematic uncertainty. We can measure this from the neutral recoil data. The beta energy in certain kinematic regimes (recoil momentum < Q/c [Kofoed-Hansen, Dan. Mat. Fys. Medd. **28**, 1 (1954)]) is uniquely defined by the recoil TOF. So the beta energy spectrum in coincidence with neutral recoils for a narrow TOF interval at long TOF will be a peak determined by the detector resolution and the angular acceptance, and a tail determined by detector response. The tail/total ratio determined in this fashion is 0.17 ± 0.03 at $E_{\beta+}$=4.0 MeV, in agreement with a GEANT calculation of 0.16, roughly half of which is from backscatter and half from bremsstrahlung. This provides sufficient accuracy for the present experiment. A detailed measurement, e.g. at Stuttgart's 0-6 MeV β^+ machine, may eventually be necessary.

A simultaneous fit of the Monte Carlo to the TOF of Ar +1, +2, and +3 charge states for $E_{\beta+}$>2.5 MeV for 1/3 of the data set is shown in Fig. 38. Fit parameters are a and a value for the uniform $\vec{E}$ field. (The trap-MCP distance is well-defined by the TOF of the fastest Ar^0 recoils.) This fit yields a=0.986±0.011(stat)± ? (syst), with a correction for non-uniform $\vec{E}$ field still necessary. Consistency between independent fits of each charge state must also be achieved – in the fit shown, they disagree at ≈2σ – and χ^2/N = 3.5.

The $\vec{E}$ field uncertainty is our largest remaining systematic error. The positions of the leading edges of the TOF spectra are sensitive to the field, independent of a, and consistent with a field 1.5% lower than our present calculations. We independently measure $\vec{E}$ using trapped stable ^{41}K atoms as test charges, by photoionizing them from the excited P3/2 level in the MOT with a pulsed (300 ps) 337 nm N_2 laser (borrowed from TRIUMF's detector facility) and measuring their TOF. This confirms the field is smaller than calculated. By moving the trapped atoms along the detector axis by adjusting a small Helmholtz coil, a rough measurement of $\frac{dE_z}{dz}$ can be achieved, and this is also consistent with the calculated field. The discrepancy between measured and calculated fields will require a correction to a of ≈0.5%, with an uncertainty to be determined. Among the problems to correct in a new field design is the shielding of all ceramics with conductors.

Search for admixture with massive ν

From the kinematic reconstruction of β^+-recoil coincidences in the present data set, we can set limits on mixing of the electron neutrino with any possible heavy neutrino for masses of ≈1–3 MeV. The kinematic signature is striking. Events would be produced near the fast recoil branch in an extra peak at longer TOF. The

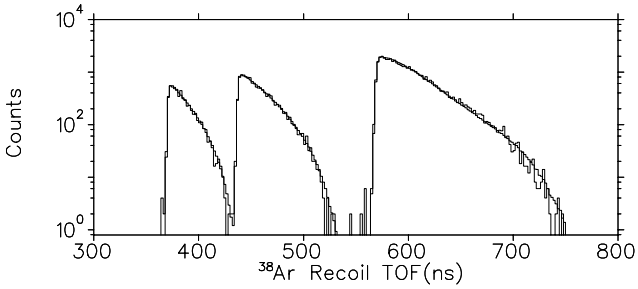

Fig. 38. Monte Carlo fit to recoil ^{38}Ar +1,+2,+3 TOF spectra, $E_{\beta+}$>2.5MeV for 1/3 of the data. See text.

present best limits in this mass range are the indirect limits from the $\pi \to e\nu$ / $\pi \to \mu\nu$ branching ratio, and vary from 1×10^{-3} for $m_\nu = 1$ MeV to 1×10^{-4} at $m_\nu = 3$ MeV [Britton *et al.*, Phys. Rev. **D46**, R885 (1992)]. The present data set should allow us to set direct limits at better than 2×10^{-3} at $m_\nu = 1$ MeV and 1×10^{-3} at $m_\nu = 2$ MeV.

The TRIUMF Theory group [McLaughlin, this Annual Report] has been investigating phenomenological signatures of ν's dwelling in compactified "large" dimensions. The limits from TRINAT may help constrain these models in this mass range.

Trapping of rubidium isotopes

Using a Nb target, ISAC is now producing large yields of Rb isotopes. For example, ≈100 times more ^{80}Rb, a reasonably clean Gamow-Teller decay, can be produced compared to ^{37}K. We trapped 5×10^6 atoms of it (limited by the data acquisition throughput). By fitting the TOF spectra assuming a Gamow-Teller decay, we deduced the Kr charge state distribution. The β^+-coincidence backgrounds from untrapped atoms ($t_{1/2} = 34$ s, similar to the trap lifetime for stable species) appear to be under control. This isotope may be useful for certain future experiments that will be statistics-limited in ^{37}K. In contrast to ^{37}K, whose isospin mirror decay allows exact calculation of recoil-order corrections, experiments in ^{80}Rb would need careful theoretical evaluation of such higher-order corrections.

No Kr^0 recoils are detected in the MCP, with an upper limit of $< 2\%$ of the Ar^0 efficiency from ^{38m}K decay, limited by accidental coincidences. This is consistent with our simple picture of our finite efficiency for Ar^0 detection being due to deexcitation of metastable noble gas atomic states. The energy release is 11.5 eV for Ar^{0*}, 9.9 eV for Kr^{0*}, and 8.3 eV for Xe^{0*}, while MCP efficiencies are known to be finite for Ar^{0*} and zero for thermal Xe^{0*} for MCPs without special coatings.

We also trapped similar quantities of ^{78}Rb. The ground state 8% decay branch of ^{78}Rb is, apparently, an isospin-forbidden Fermi transition [Bavaria *et al.*, Z. Phys. **A302**, 329 (1981)]. (This requires the parity of the ^{78}Rb ground state to be +, which is probably so but remains uncertain.) Although the $\log(ft_{1/2}) = 7.9$ is slow, deviations from $a = 1$ could signal a scalar interaction. We have tested the feasibility of measuring the ^{78}Rb β-ν correlation, but the 17.7 minute half-life and background from many excited state branches make measurements very difficult.

By measuring the trap frequency response to this I = 0 nucleus, we were able to optimize the trap parameters and calibrate the trap. We then attempted to trap the $t_{1/2} = 60$ ms isotope ^{74}Rb, in hopes of measuring its isotope shift and deducing the charge radius. Scanning the most likely 0.1 fm^2 region, an ≈2σ significant peak in the β^+ telescope, along with a single clean β^+-recoil coincident event, were seen. However, this is inadequate for publication.

Optical pumping

An off-line lab has been started to work on optical pumping of stable ^{41}K, to prepare for experiments with polarized ^{37}K. The present strategy will be to turn off the MOT (whose 6 beams scramble the polarization) and optically pump the atoms as the cloud expands. A possible measurement cycle (of 5 ms duration) would be the following: trap ^{41}K or ^{37}K atoms in a MOT; turn off the MOT light and B field; optically pump the atoms with D1 light (≈10 μs); count for 5 ms (or probe the polarization, with cycles interleaved) as the cloud falls and expands, and restore the MOT. During the measurement the cloud would fall 0.1 mm and expand 8 mm at a temperature of 1 mK. We have measured our present trap temperature to be 0.5–1 mK for ^{41}K; it is known that in a MOT with different laser detunings 0.2 mK can be achieved in K [Williamson and Walker, JOSA **B12**, 1393 (1995)]. Detailed calculations of optical pumping at arbitrary B field (made non-trivial by the small hyperfine splitting) have been performed, and polarizations greater than 99% can be achieved in this fashion.

The polarization probing method must have less dependence on circular polarization than the optical pumping process. This can be achieved by using stimulated Raman scattering to move atoms from specific magnetic sublevels to the other hyperfine-split ground state manifold, and then detect them by on-resonant fluorescence. We have calculated such a Raman pumping/resonant probing scheme. The two Raman beams must be copropagating to avoid Doppler shifts, and a configuration of two linearly polarized beams ("$\pi \perp$ lin") can be used. The Raman beams are at 90 degrees to the optical pumping axis. The Raman beams have sufficient frequency resolution to resolve the magnetic sublevels by using a weak magnetic field. After the atoms have been moved to the other hyperfine manifold, they can then be detected by D1 light on-resonant fluorescence probing.

Due to the narrow hyperfine splitting of ^{37}K, only a few photons per cycle per atom will be produced. By gating the phototube data acquisition to look only during the 200 ns needed to probe the atoms per cycle, more than sufficient signal/noise for 1,000 atoms in the trap can nevertheless be achieved, with expected count rates of 500 Hz in a realistic detector geometry.

The better the polarization achieved, the less accuracy is required in probing the magnetic sublevels. Calculations suggest 99% polarization can be achieved, thus requiring ≈10% accuracy measurements of the

other magnetic sublevel populations to achieve 0.1% polarization knowledge required. (If that population is in the most likely contaminant sublevel, F=2 M_F=1, the nuclear polarization of that state is still 5/6, so the degradation of the nuclear polarization is small.)

NCE photonics innovations

TRINAT is now part of the neutral atoms trap section of the (Network of Centres of Excellence) Canadian Institute for Photonic Innovations, which is intended to encourage collaborations between disparate groups. Through student and postdoc visits, expertise will be shared with atomic physics groups at Toronto and York. William van Wijngaarden's group at York is working on a lifetime measurement of trapped Cs atoms that requires isolation of one magnetic sublevel, and techniques of optical pumping and stimulated Raman transitions will be common to both projects. Aephraim Steinberg's group at Toronto is pursuing a number of fundamental quantum mechanics measurements using MOTs.

Experiment 719
^{4}He(π^+,π^-pp) invariant mass measurement with CHAOS

(R. Meier, Tübingen; M.E. Sevior, Melbourne; G.R. Smith, TRIUMF)

This experiment received beam time during the high intensity running periods in 1996. The CHAOS spectrometer with a ^{4}He gas target was used on the TRIUMF M11 beam line. Measurements were performed at pion kinetic energies of 115 MeV and 105 MeV.

The aim of the experiment was to search for the hypothetical d' dibaryon, which is a possible explanation for the enhancement observed in the total cross section of pion double charge exchange (DCX) to discrete final states in nuclei around $T_\pi = 50$ MeV. From the analysis of DCX, the mass of the d' has been derived to be about 2065 MeV, with a width of about 0.5 MeV. The quantum numbers were suggested to be $J^\pi = 0^-$ and $T = 0{,}2$. With these quantum numbers, the d' cannot couple to the two nucleon channel, but will decay into a pion and two nucleons.

Experiment 719 searches for the d' by investigating the double charge exchange reaction π^+ ^{4}He $\rightarrow$ π^-pppp. If the d' exists, a large part of the DCX cross section in the region above the d' production threshold should be due to the reaction π^+ ^{4}He $\rightarrow$ $d'pp$ $\rightarrow$ π^-pppp.

CHAOS was configured to simultaneously detect the π^- and at least two protons. From the measured momenta of the three detected particles, the invariant mass of the π^-pp system can be calculated; the d' should show up as a peak in the invariant mass spectrum. As only one of the four protons in the final state can possibly come from the d', the peak will be accompanied by a combinatorial background from detecting one or two protons not from the d'. Additionally, there will be background from non-resonant DCX.

Although the DCX mechanism via the d' is predicted to dominate the DCX cross section just above the d' threshold (at about $T_\pi = 80$ MeV), the measurements were done at 25 and 35 MeV above threshold. Simulations showed that near threshold, the signature for the d' is indistinguishable from the behaviour of conventional DCX. This is because both conventional DCX and the d' invariant mass distributions peak at the same place due to acceptance constraints just about threshold.

Final results

Data analysis for this experiment has been completed and forms the Ph.D. thesis of Melbourne student John Clark. The thesis was submitted for examination in December.

The top two histograms in Fig. 39 show the results for the invariant mass spectra constructed from the momenta of the detected π^- and two protons together with the simulation predictions. For the d' mechanism, shown as the solid double line, a peak at the invariant mass of the d' is expected. However, since there are four protons in the final state, the peak is accompanied by a combinatorial background from detecting one or two of the protons which are not from the d'. Non-resonant DCX was modelled by the processes of two sequential single exchange ((π^+,π^0) (π^0,π^-)) reactions (SSCX), which produces a continuous distribution of the invariant mass, shown by the solid single line. The dotted line shows the curve for five-body phase space. The data points are also shown with statistical error bars. All the curves are fitted to the data using a least-squares method.

To extract the relative contributions of the two simulated mechanisms necessary to describe the data, the invariant mass spectra were fit with the curves from the simulation. From this fit, the fraction of events attributed to each mechanism was found. These fractions were then corrected for the different acceptances for the mechanisms.

For the 115 MeV data no d' contribution was required in the best fit but a d' contribution of 34% was allowed at a 90% confidence level. The 105 MeV data required a 4% dibaryon contribution in the best fit. However, at this energy the data could hardly distinguish between the models at the 90% confidence level (a dibaryon contribution of up to 92% was allowed), so the hypothesis that the d' mechanism is wholly responsible for the data at this energy cannot be rejected.

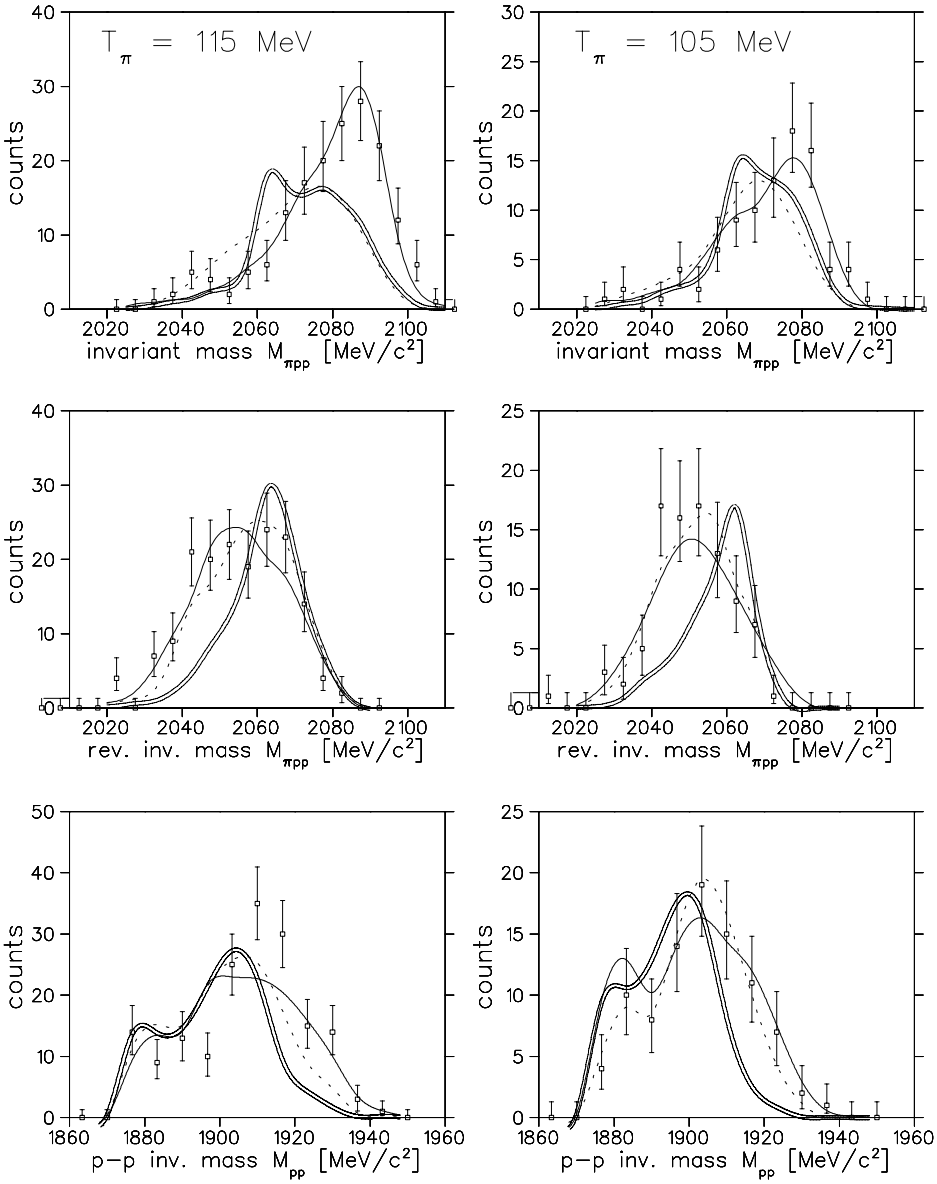

Fig. 39. The invariant mass of the observed pion and two protons is shown in the top histograms, the "reverse" invariant mass in the middle histograms and the invariant mass of the two protons in the bottom histograms. The histograms on the left are for T_π=115 MeV and those on the right are for T_π=105 MeV. The lines show simulation results from the dibaryon mechanism (double solid line); the conventional (SSCX) mechanism (single solid line); five-body phase space (dotted line).

The invariant mass distribution can also be determined using the π^- and two protons *not* observed by calculating the missing invariant mass in the reaction (the middle histograms in Fig. 39). Again, the SSCX model adequately explained the data at both energies. For the 105 MeV data, a stronger discrimination at this energy can be made using this spectrum than using the "direct" invariant mass. In this spectrum, the difference between the two models is more pronounced which makes it more suitable for examining whether the d' contributes to the DCX process. Since no evidence for d' was found, a tighter limit may be placed on d' production: a d' contribution of 1% was required in the best fit, and up to 39% at the 90% confidence limit.

The invariant mass of the two observed protons is also measured (bottom spectra in Fig. 39), providing a measure of the FSI of the d' decay, which would cause the decay protons to tend to a small relative momentum and result in a peak at low invariant mass. At both energies the SSCX mechanism performs significantly better than the dibaryon mechanism.

It is noted that the d' does not make a significant contribution in the best fit in any of the graphs. It is also noted that the SSCX with FSI model adequately

Table VII. Results of dibaryon search showing the calculated χ^2 values for the fits of the data to the two competing models, as well as the d' contribution for the combination of the two models which produces the lowest χ^2 value, and the d' contribution upper limit at the 90% confidence interval. These values are tabulated for the three different observables: the invariant mass, $M_{\pi pp}$, the "reverse" invariant mass, $M_{\pi pp}$ (rev), and the invariant mass of the two protons, M_{pp}.

	115 MeV				105 MeV			
	χ^2/df		d' fraction		χ^2/df		d' fraction	
	SSCX	d'	best fit	90% CI	SSCX	d'	best fit	90% CI
$M_{\pi pp}$	0.7	5.0	0.00	0.34	0.8	1.6	0.04	0.92
$M_{\pi pp}$ (rev)	1.2	3.9	0.12	0.42	0.9	3.4	0.01	0.39
M_{pp}	2.2	5.2	0.00	0.00	0.6	3.0	0.00	0.53

describes all the data with the exception of the proton-proton invariant mass histogram at $T_\pi = 115$ MeV, but here the d' does not improve the situation. This flat structure at low M_{pp}, also hinted at in the $T_\pi = 105$ MeV data, provides the greatest discrepancy between the data and our model, and so it may provide the most insights into improving our reaction mechanism.

The results of the fits are tabulated in Table VII.

Conclusions

The DCX reaction on ^{4}He has been studied semi-exclusively with the CHAOS set-up by detecting two of the four outgoing protons in addition to the outgoing negative pion. The resulting invariant mass spectra exhibit details of the reaction mechanism. The data for $M_{\pi pp}$ and M_{pp}, which are particularly suited to search for signatures of possible d' production in this reaction, are consistent with d' contributions substantially smaller than predicted. The SSCX Monte Carlo simulations describe the new experimental data satisfactorily without requiring a large d' contribution, as anticipated from the analysis of the total cross sections.

A paper describing these results is in the final stages of preparation before submission to a scientific journal.

Experiment 723
Study of pion-nucleus double-scattering reactions
(R. Tacik, TRIUMF/Regina)

This experiment was run in the M11 pion channel at TRIUMF. A thin rod of plastic scintillator was used as an active carbon target. The CHAOS spectrometer was used to measure the angles and momenta of outgoing particles. The CHAOS first and second level triggers were set to accept ≥ 2 charged particles, thus enabling the investigation of a large number of reactions simultaneously. Data were obtained with incident pions of both polarities. In the case of π^+, measurements were performed at incident energies of 120, 160, 200, 240, and 280 MeV. For π^-, at 200, 240, and 280 MeV.

One aim of the experiment was to study the previously unmeasured pion two-nucleon knockout reactions: (a) ^{12}C(π^+,π^+pp), (b) ^{12}C(π^+,π^-pp), and (c) ^{12}C(π^-,π^-pp). The simplest mechanism for these reactions is that of two sequential quasi-free scatterings, i.e. $\pi^+p \to \pi^+p$, $\pi^+p \to \pi^+p$; $\pi^+n \to \pi^\circ p$, $\pi^\circ n \to \pi^-p$; or $\pi^-p \to \pi^-p$, $\pi^-p \to \pi^-p$, for reactions (a), (b), and (c) respectively. Since the ratio of these elementary reactions is 9:2:1 for resonance energy pions, we expected to observe about 81:4:1 for the ratio of the three two-nucleon knockout reactions, possibly modified somewhat due to interference with Δ-nucleon knockout processes. In fact, at $T_\pi = 240$ and 280 MeV, the measured ratio was roughly 5:1:1. This is a surprising result.

The measured energy dependence of the (π^+,π^+pp) reaction can be described reasonably well by a Monte Carlo model based on the sequential scattering mechanism. The same model seriously underpredicts the yields for the (π^+,π^-pp) and (π^-,π^-pp) reactions. It may be interesting to note that a similar observation was made by Morris *et al.* [Phys. Lett. **B419**, 25 (1998)] in the case of the ^{12}C$(\pi^+,\pi^\pm p)$ reactions at T_π = 500 MeV. Morris *et al.* found that an intra-nuclear cascade model reproduced their (π^+,π^+p) data, but underpredicted the (π^+,π^-p) cross sections by a large factor. Morris *et al.* attributed the difference to quasi-free scattering from the Δ^- component of the nuclear ground state wave function. If that were the explanation for our case, we would expect it to show up strongly in a comparison of the measured distributions for the (π^+,π^-p) and (π^+,π^-pp) reactions, since the former could proceed via the two-body mechanism $\pi^+\Delta^- \to \pi^-p$. We do not see any evidence for a two-body mechanism in the double-charge reactions, and in fact, as discussed below, we do see evidence that both the (π^+,π^-pp) and the (π^-,π^-pp) reactions involve an additional undetected nucleon.

Figure 40 shows the summed energy distributions for the three two-nucleon knockout reactions measured at $T_\pi = 280$ MeV. The dashed lines indicate the maximum energy assuming that only the detected particles were involved in the reaction, and that the residual nucleus was left in its ground state. In the case of (π^+,π^+pp), the bulk of the events have relatively little missing energy. For the other two reactions, the distributions show substantially more missing energy.

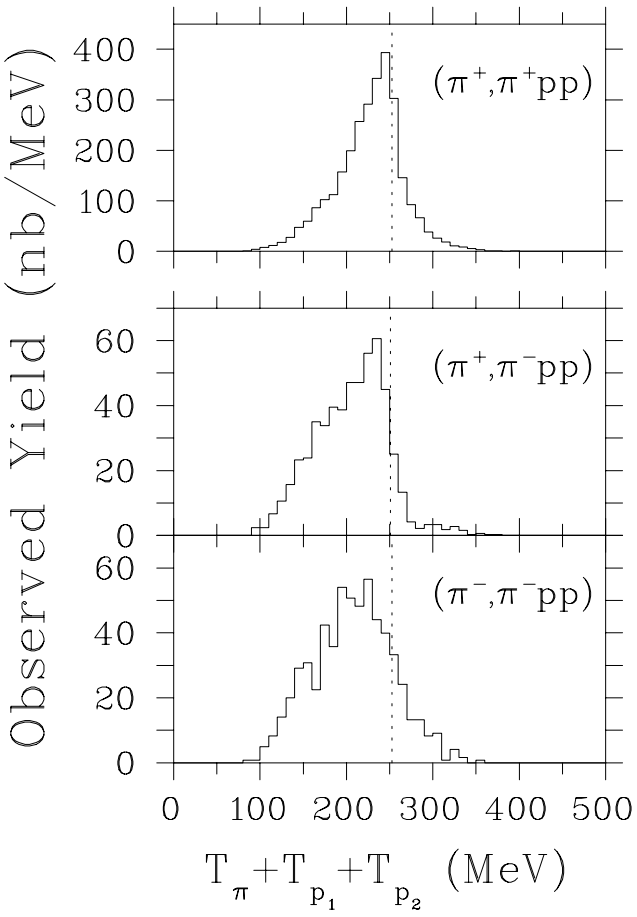

Fig. 40. Normalized summed energy distributions measured in Expt. 723.

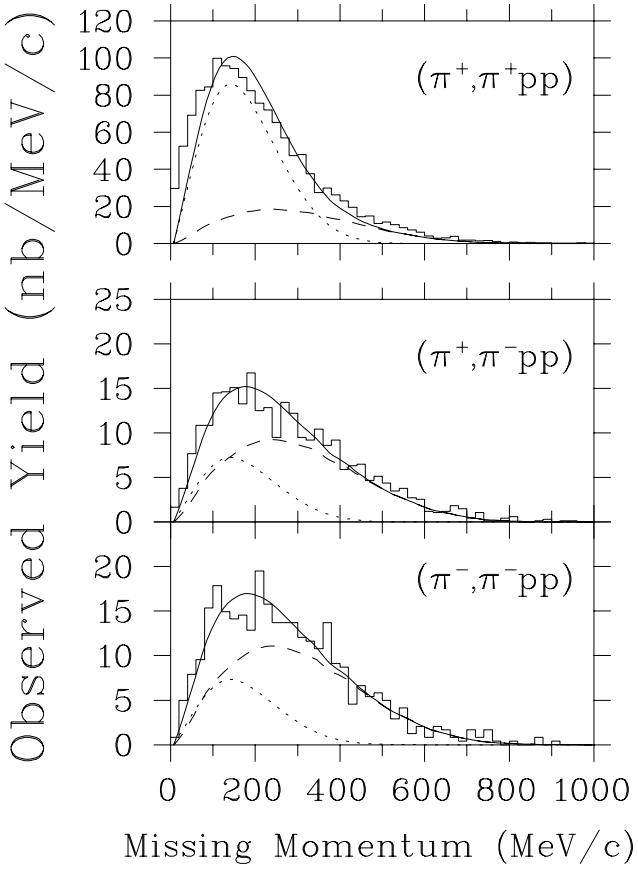

Fig. 41. Normalized missing momentum distributions measured in Expt. 723. The histograms represent the data, while the various lines represent the results of model calculations. See text for details.

Figure 41 shows the missing momentum distributions for the three reactions, also at $T_\pi = 280$ MeV. In this figure, the dotted lines represent the results of a Monte Carlo model in which only the three detected particles participated. In this case, the missing momentum is due to the initial Fermi momentum of the two participating nucleons, which is carried away by the recoiling residual nucleus. The dashed lines show the results of a Monte Carlo model in which there was an additional undetected nucleon participating in the reaction. The solid line is the 'best fit' result obtained by varying the magnitudes of the dotted and dashed curves and summing them. This analysis supports the idea that the sequential scattering mechanism is responsible for most of the observed (π^+, π^+pp) cross section, but that some different mechanism is dominant in the case of the other two reactions. Note that models in which there are two or more undetected nucleons do not describe the data very well.

The (π^+, π^-pp) and (π^-, π^-pp) reactions are similar in more than just total observed yield. For example, the shapes of the measured momentum and angular distributions, for both π^-'s and p's, for both reactions, are quite similar. This implies that the same mechanism might be responsible for both. Further modelling is still in progress to try to identify just what that mechanism is, and to determine, from a comparison with other measured reaction channels, how often the undetected nucleon is a proton and how often it is a neutron. One interesting possibility is that the reaction mechanism might involve double-Δ excitation. This could have far-reaching consequences. It would certainly have a bearing on the results of CHAOS Expt. 722 [Tacik *et al.*, Phys. Rev. **C57**, 1295 (1998)], where it was found that the dominant mechanism responsible for the ^{12}C(π^+, ppp) pion absorption reaction involved four nucleons, and not just the three which were detected.

Experiment 741
Beta-delayed proton decay of ^{17}Ne to α-emitting states in ^{16}O
(J.D. King, Toronto)

The goal of this experiment is to obtain an α-particle spectrum from the break-up of ^{16}O following the β-delayed proton decay of ^{17}Ne, and to use this spectrum to reduce the uncertainty in the ^{12}C$(\alpha, \gamma)^{16}$O

reaction rate, which is of prime importance in determining the ratio of ^{16}O to ^{12}C at the end of helium burning in stars. In Expt. 589 we measured the α-particle spectrum from the break-up of ^{16}O following the β decay of ^{16}N. Through simultaneous R- and K-matrix fits to this spectrum, to the ^{12}C$(\alpha,\gamma)^{16}$O data sets, and to ^{12}C(α,α) scattering data, we were able to reduce considerably the uncertainty in the $E1$ component of the astrophysical S-factor for the ^{12}C$(\alpha,\gamma)^{16}$O reaction, which is determined primarily by the tail of the sub-threshold 1^- state at 7.117 MeV. Since the 2^+ state at 6.917 MeV is not populated in the decay of ^{16}N, the effect of the tail of this sub-threshold state on the $E2$ component was not determined, and a very large uncertainty in this component, which could be as large as the $E1$, still exists. However, 2^+ states in ^{16}O are populated in the β-delayed proton decay of ^{17}Ne and the feasibility of using this decay is being explored in this experiment.

In last year's report we described the preliminary results of a study of the three-particle break-up of ^{17}Ne through the isobaric analogue state (IAS) of ^{17}F via proton decay to the 9.59 MeV state in ^{16}O, and via α decay to excited states in ^{13}N. A new software procedure has been developed to investigate the kinematics of triple coincidence events on an event-by-event basis; it replaces the procedure described in last year's report and is outlined below. Data from the runs of November and December, 1998 (described at the end of last year's report) have been analysed. An experimental run in April, 1999 was designed to produce a high-quality α-particle spectrum. In this report we will review the present status of data on β-delayed particle decay of ^{17}F.

Kinematic procedure

The objective is to discriminate against background by eliminating events which are not kinematically reasonable based on the observed energy and position information. Briefly, the procedure is as follows:

i) the energies of all three particles are set as variables;

ii) the proton–α and proton–^{12}C angles are computed from the values of the fitted energies (the α–^{12}C angle does not give another constraint since the three angles should add up to 360 degrees);

iii) the angles computed in ii) are compared with those between the centres of the detector elements;

iv) the sum of the fitted energies is computed (this is a good constraint since we know more than 99.9% of the triples are from the IAS).

This procedure produces a function consisting of 6 terms of the form $((v(\mathrm{obs})-v)/\sigma)^2$ where $v(\mathrm{obs})$ is the observed value, and v is the fitted or calculated value. The value of the function is returned as the average of the six terms. The result shows that for most events with energy sum around 3.43 MeV, the value of the function is less than unity, indicating that the values of σ used in the fitting are reasonable.

November/December, 1998 run

In November and December, 1998 the break-up of the IAS in ^{17}F was studied with an improved experimental arrangement shown in Fig. 42. The DSSD and PIPS detectors were moved back to 10 cm from the collector foil, and scintillator paddles were placed just outside the detector array so that they subtended a solid angle of about 25% of 4π at the collector foil. Moving back the detectors reduced the solid angle subtended by each detector element, while the presence of the scintillators meant that a quadruple coincidence (β–p–α–^{12}C) could be obtained with reasonable efficiency. In addition, a 1,500 μm thick Si detector was placed at a distance of 20 cm from the collector foil beyond the DSSDs and at a small angle to the beam direction. The purpose of this detector was two-fold: to

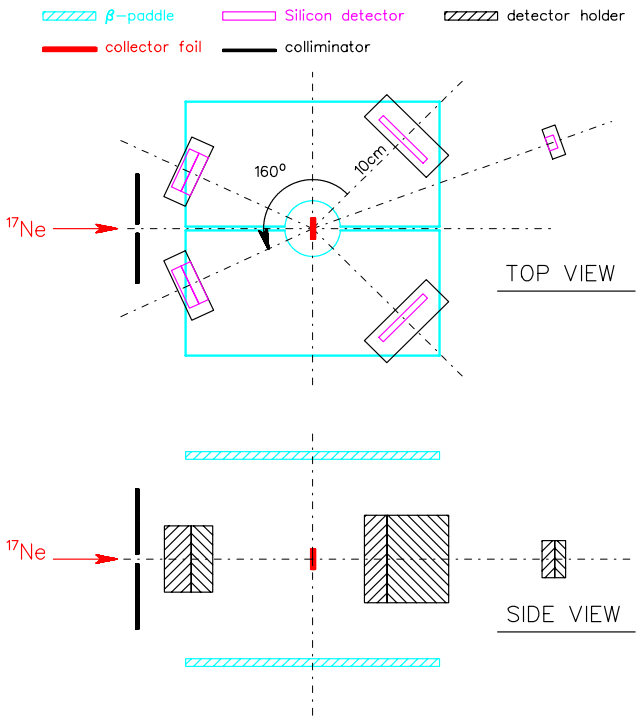

Fig. 42. Set-up for Nov/Dec, 1998 run using double-sided strip detectors for protons and alphas and PIPS detectors for ^{16}O and ^{13}N recoils. A 1500 μm detector was placed at 20 cm from the collector foil to accumulate a high-quality proton spectrum.

accumulate low-energy particle spectra in which protons and α's could be separated by time of flight using a start signal from one of the scintillator paddles; and to obtain a high quality spectrum of the weak proton groups at energies greater than 8 MeV. Some details of the ^{17}F decay scheme were still uncertain, particularly because of overlap between low-energy proton and α groups which were both obscured by the tail of the passage of the intense β flux through the various detectors used in previous runs.

The results from this run were not as useful as anticipated for two main reasons.

1. The time resolution of 3 ns from the DSSDs is adequate to allow separation of α and proton groups in the DSSDs below an energy of 3 MeV. However, the time resolution with the PIPS detectors of about 15 ns resulted in a much larger background in the coincidence spectra than had been expected.

2. The yield of ^{17}Ne from TISOL, although initially $> 10^5$ s^{-1}, decreased steadily during the run to near 10^4 s^{-1}. With the reduced detector solid angle due to moving the detectors farther from the collector foil, this relatively low ^{17}Ne beam meant that far fewer triple and quadruple coincidences were obtained than had been expected.

The rather poor timing resolution and relatively low ^{17}Ne yield means that, while cleaner triple sum and derived α spectra than those obtained previously were obtained, they did not reach the purity expected and they contained significantly fewer counts than previous runs. A much bigger improvement in background level in the triple sum spectrum resulted from the smaller solid angle subtended by each pixel in the DSSDs than from the implementation of an additional β-coincidence requirement. The triple-coincidence α spectrum is shown in Fig. 43.

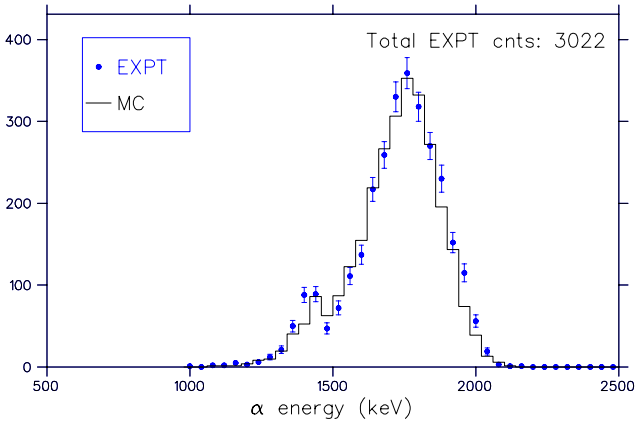

Fig. 43. Final triple-coincidence α spectrum. The histogram is the result of a Monte Carlo calculation using a modified R-matrix approach.

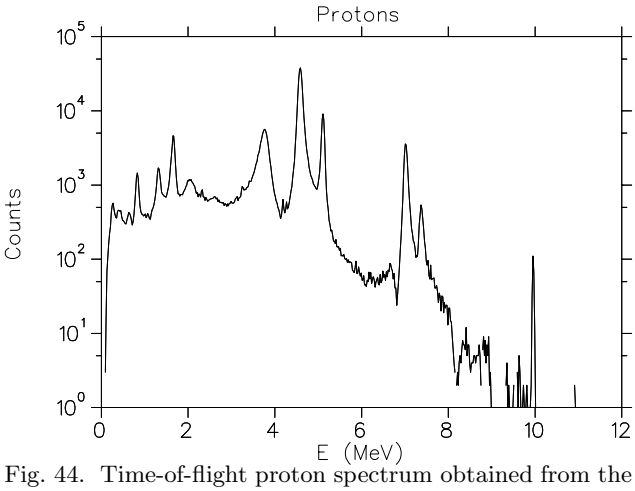

Fig. 44. Time-of-flight proton spectrum obtained from the 1500 μm detector.

Proton spectrum

The proton spectrum from the 1500 μm detector obtained by applying a time-of-flight condition is shown in Fig. 44. Of particular interest is the lowest-energy peak in the spectrum which is rather broad and flat-topped. It is due to protons from the break-up of the 2.365 MeV state of ^{13}N into ^{12}C plus a proton following the α decay of the IAS of ^{17}F. The energy available is 0.42 MeV, but the decay is from a recoiling ^{13}N nucleus which broadens the peak. This complicated spectrum is being analyzed using Breit-Wigner peak shapes with energy-dependent widths and interference between transitions from ^{17}F states with the same width and parity, in conjunction with a similar analysis of the singles α particle spectrum described below.

Singles alpha spectrum

It was not possible to obtain a high quality α spectrum from the 1500 μm detector because of random background due to the strong ground state proton transitions which could not be eliminated from the spectrum. An experimental run in April, 1999 was designed to produce a high purity α spectrum and to put an upper limit on the α-decay branch from the 9.45 MeV state in ^{17}F to the 2.365 MeV state in ^{13}N. Alpha particles from this decay have a cm energy of about 0.95 MeV. If such a branch were to have sufficient strength, the α particles, which would have energies in the same range as α's from the tail of the 6.917 MeV state in ^{16}O populated by proton decay from the 9.45 MeV state, would interfere with measurement of α's from the tail since they would also be in coincidence with a proton and ^{12}C recoil after break-up of the 2.365 MeV state. The experimental set-up is shown in Fig. 45. The spectrum of α particles in coincidence with recoiling ^{13}N nuclei is shown in Fig. 46. The

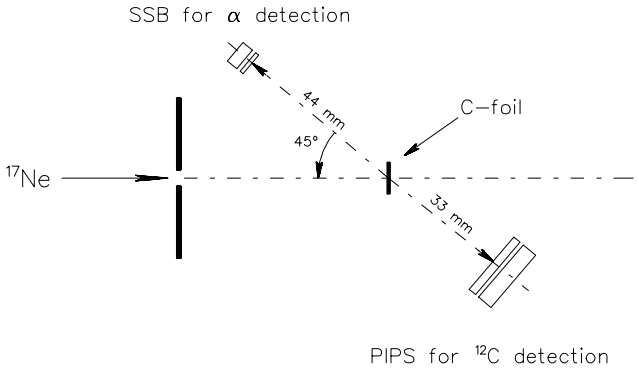

Fig. 45. Experimental arrangement for obtaining an α particle spectrum free from proton contamination.

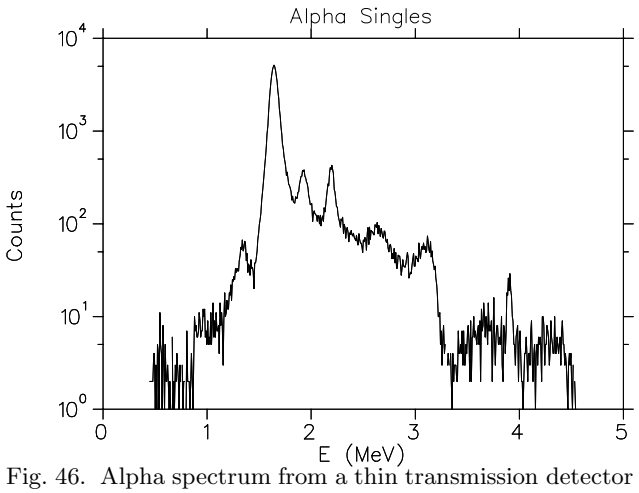

Fig. 46. Alpha spectrum from a thin transmission detector after applying a ratio cut.

ratio technique has been used to remove background from electron and proton pile-up. An upper limit of 0.004 has been determined for the strength of the 9.45 $\rightarrow$ 2.365 transition relative to the 9.45 $\rightarrow$ 6.917 proton transition.

Detailed analysis of the proton spectrum of Fig. 44 and the α spectrum of Fig. 46 using the Breit-Wigner fitting techniques is nearing completion. The results will supply energies, widths and particle-decay branching ratios for unbound states in ^{17}F from 8.08 to 11.193 MeV.

Experiment 766
The ortho-para transition rate in muonic molecular hydrogen
(D.S. Armstrong, William & Mary; T.P. Gorringe, Kentucky)

Muon capture has long been recognized as a useful probe of the semileptonic weak interaction. The elusive pseudoscalar coupling g_p for the proton, in particular, can be measured using μ^- capture. While the theoretical expectation for the value of g_p appears robust (chiral perturbation theory results match the older current algebra predictions), the experimental situation is not as clear. The two most recent and most precise measurements for the proton appear to disagree with each other. The radiative muon capture (RMC) experiment (TRIUMF Expt. 452) [Wright *et al.*, Phys. Rev. **C57**, 373 (1998)] yields a much larger value for g_p than does the late-1970's measurement from Saclay [Bardin *et al.*, Phys. Lett. **104B**, 320 (1981)], which used ordinary, non-radiative muon capture (OMC). However, both experiments used liquid hydrogen targets, and their interpretation in terms of weak couplings requires knowledge of the relative population of the muonic atomic and molecular states. In particular, λ_{op}, the transition rate between the ortho and para states of the $p\mu p$ molecule, needs to be known with precision. The extracted value of g_p is changed drastically (especially for the case of the OMC experiment) depending on the value of λ_{op} assumed – see Fig. 47.

The $p\mu p$ molecule is formed almost entirely in the (excited) ortho-molecular state, and (if the muon doesn't itself decay, or get absorbed by the proton) can decay to the para-molecular ground state. This decay rate (λ_{op}) is expected to be rather slow; the best theoretical prediction $\lambda_{op} = (7.1 \pm 1.2) \times 10^4$ s^{-1} [Bakalov *et al.*, Nucl. Phys. **A384**, 302 (1982)] is not in good agreement with the only previous measurement which yielded [Bardin *et al.*, *op. cit.*] $\lambda_{op} = (4.1 \pm 1.4) \times 10^4$ s^{-1}. Thus, a new measurement of λ_{op} is needed to clarify the situation.

The present experiment accesses λ_{op} by measuring the time distribution of neutrons following μ^- capture in the target ($\mu^- + p \rightarrow \nu_\mu + n$). Due to the different combinations of hyperfine muonic atomic states that make up the ortho and para molecules, and the spin-dependence of the weak interaction, muon capture proceeds more rapidly from the ortho state ($\lambda_o \sim 600$ s^{-1}) than the para state ($\lambda_p \sim 200$ s^{-1}). Thus the

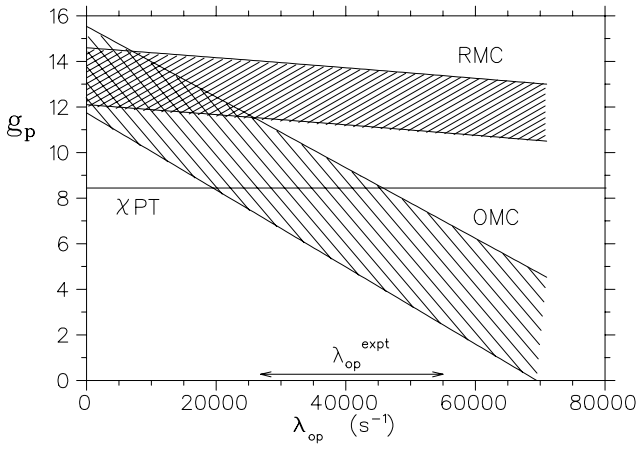

Fig. 47. The pseudoscalar coupling g_p from radiative (RMC) and ordinary (OMC) muon capture experiments vs. λ_{op}. χPT indicates the chiral perturbation theory prediction.

time-dependence (relative to the arrival of the μ^- in the target) of the neutrons produced is not a simple exponential, but is modified by the ortho-para conversion. A fit to the time distribution allows λ_{op} to be extracted, and avoids the difficulty of determining the absolute neutron detection efficiency.

Five liquid scintillation detectors were used to detect the monoenergetic 5.2 MeV neutrons from μ^- capture on the proton. These detectors surrounded the liquid hydrogen target which was originally used in the RMC experiment; the hydrogen is isotopically enriched protium (< 0.5 ppm deuterium content) to eliminate complications due to muon transfer to heavier isotopes. Plastic scintillators placed between the detectors and target allowed discrimination between neutrons and electrons from muon decay. Two independent levels of pulse-shape discrimination (PSD) in hardware and software were applied to separate neutrons from photons in the liquid scintillators. A pair of plastic scintillators in a telescope identified muons incident on the target.

The combination of TRIUMF's high duty factor and the use of multihit electronics allows us to avoid having to reject "pileup" muons. The arrival time was digitized for every muon arriving in a 32 μs window before the time of the neutron. Thus muon pileup causes a perfectly flat background to the time spectrum, and cannot cause a distortion to the time fit. Similarly, the (large) cyclotron-induced background of neutrons produced elsewhere than the target also creates a flat background, since they are uncorrelated with a muon passing through the beam scintillators.

The only backgrounds that can produce anything other than a flat contribution to the time spectrum are 1) muon capture on the target walls, 2) muons that pass through the beam telescope but fail to enter the target, and 3) photons from the target that either sneak through the PSD or produce real neutrons through (γ, n) reactions. The target walls are made of Au and Ag so μ^-'s stopped there are rapidly captured, thus the background is eliminated by a cut rejecting the first ~500 ns of the time spectrum. The second background (primarily muon capture in the final beam scintillator) was measured via empty-target runs and found to be manageable. The final background was measured by separate runs with a μ^+ beam. The primary source of photons from the target (aside from muonic X-rays, which are rejected via a prompt timing cut) is from bremsstrahlung of decay electrons, so the background remains the same for a μ^+ beam while the signal (muon capture) disappears. Again, the background was found to be manageable.

The 5.2 MeV neutron signal from a typical liquid scintillator is shown in Fig. 48. Electron-rejection and

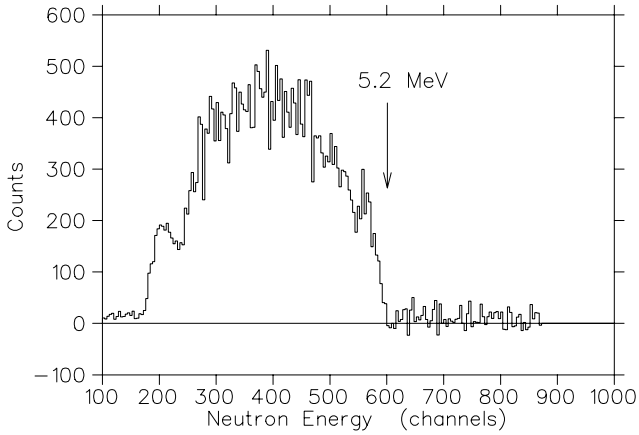

Fig. 48. Typical neutron energy spectrum.

PSD cuts have been applied, and an out-of-time background subtraction has been performed. The characteristic "box" shape of the liquid scintillator response to a monoenergetic neutron is clearly seen. The time-distribution of events in the correct energy window is shown in Fig. 49, after the 500 ns wall-background cut has been applied. The ~2 μs lifetime hydrogen muon capture component is seen, superimposed on a time-independent background, as described above. Optimization of the various cuts has not yet been completed; however, preliminary fits indicate that λ_{op} should be able to be extracted from the time spectrum.

Data were taken in two periods (June and November) for a total of 3 weeks of beam. These data are under detailed analysis and the results will form the basis for the Ph.D. thesis of J.H.D. Clark (William & Mary).

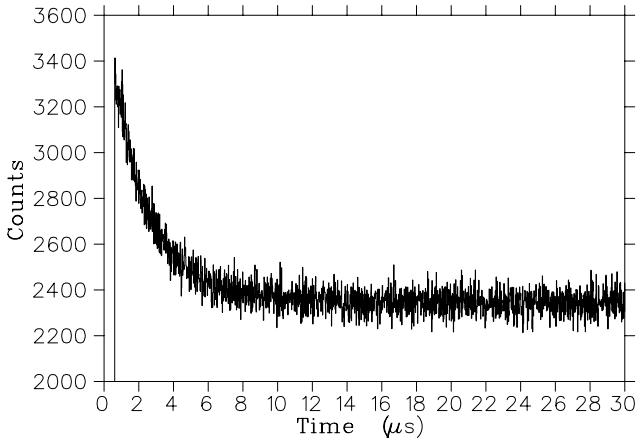

Fig. 49. Time spectrum of neutrons from μ^- capture on protium, after PSD, neutron energy, and wall-background cuts.

Experiment 778
$\pi^{\pm}p$ differential cross sections in the region of Coulomb nuclear interference
(K.J. Raywood, G.R. Smith, TRIUMF)

Introduction

The primary goals of the CHAOS physics program to date have been to test predictions and measure parameters of chiral perturbation theory. To this end, measurements have been made in the $\pi^{\pm}p$ sector of pion induced pion production (Expt. 624) and elastic scattering analyzing powers (Expt. 560). Experiment 778 deals with the next stage of this program: the measurement of $\pi^{\pm}p$ absolute differential cross sections at very forward angles where Coulomb scattering interferes destructively (constructively) with $\pi^{+}p$ ($\pi^{-}p$) hadronic scattering amplitudes.

These data will be used to determine, to a precision of a few per cent, the real part of the isospin-even scattering amplitude, D^{+}, at $t = 0$. This information is missing in the current partial wave analyses. Its inclusion will greatly improve the determination of the πN scattering amplitudes. As a result, it will improve the determination of the πN coupling constant, the πN scattering lengths, and the πN Σ term; all observables of crucial importance.

The Σ term, in particular, is a fundamental quantity. It is a direct measure of chiral symmetry breaking and can be used to determine the strange quark content of the proton. It can be obtained experimentally from the isospin-even S- and P-wave scattering lengths $a^{+}_{0^{+}}$ and $a^{+}_{1^{+}}$. A systematic set of measurements in the region of Coulomb nuclear interference (CNI) can be used to directly measure these scattering lengths and thus provide a value of $\Sigma_{\pi N}$ that is less dependent on the results of partial wave analysis than previous determinations.

The experimental goal is to provide differential cross sections of $\pi^{\pm}p$ elastic scattering at pion bombarding energies between 20 and 70 MeV. The precision of the measurements must be no greater than 5% and the angular range should extend down to about 5°, thus presenting a considerable experimental challenge.

Experiment

In addition to the CHAOS spectrometer, the CNI experiment requires two specialized pieces of equipment. A π/μ particle identification range stack is placed so that it accepts particles scattered at small angles. It covers the scattering angle range from about 5° to 30° and is necessary in order to distinguish elastically scattered pions from $\pi \rightarrow \mu\nu$ decays in the target region. The experimental layout is shown in Fig. 50. The first layer of the stack consists of eight side by side scintillator paddles, each subtending about 3° in scattering angle. The five subsequent layers each consist of two large scintillator paddles, one above the other. All scintillators are viewed by phototubes at both ends. Aluminum sheets are placed between the scintillator layers to *range out* pions two layers earlier than muons with the same momentum. The π/μ stack was built in 1998 and first used that same year. In 1999, the mechanism for raising and lowering the large aluminum sheets (up to about 25 kg) was improved and the stack continued to operate well.

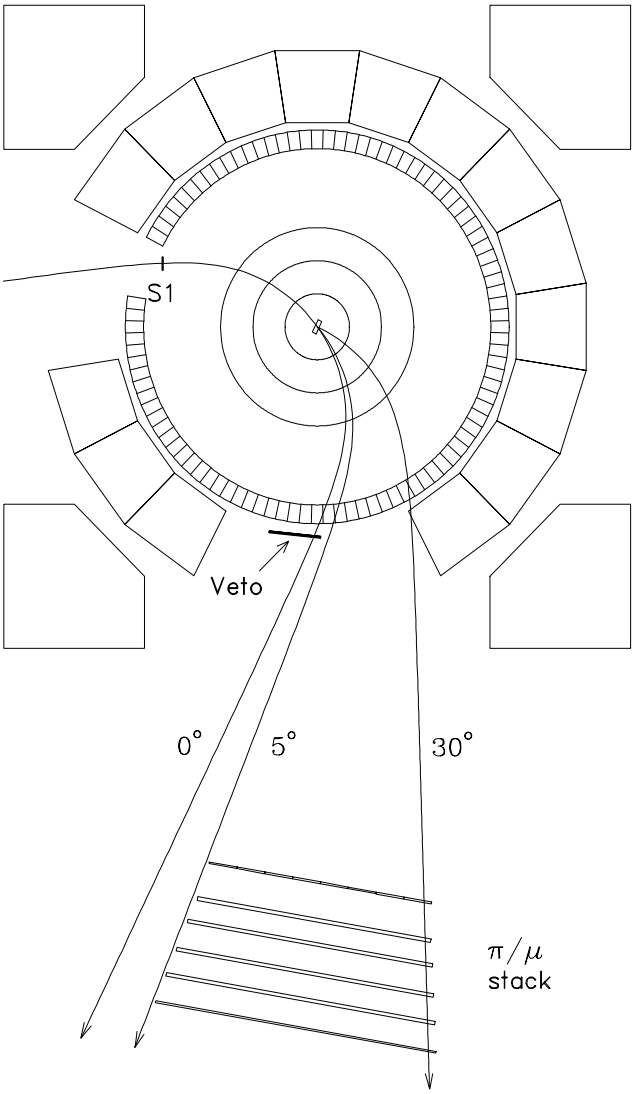

Fig. 50. The layout of the experiment. The CHAOS magnetic field is perpendicular to the page. The central beam trajectory is labelled as 0° and the angular acceptance of the π/μ stack is indicated by the tracks with 5° and 30° scattering angles.

The other special piece of equipment required for CNI is a planar cryogenic LH_2 target. Following the disappointments of 1998, when the target failed to operate, a new target was constructed by the Cryogenic Targets Group over the winter (98/99). It was designed

to allow the planar target cell to be replaced quickly in order to use different thicknesses. The target was ready about three weeks into the first high intensity period of the year (April/May). A 20 mm thick cell was used with a beam energy of 45 MeV for the remainder of the period. During the fall, 1999 high intensity period, the target was again used successfully, this time with a 12.5 mm thick cell and beam energies of 45 and 26 MeV. At one stage, the 8 μm thick cell windows failed (without damaging the outer windows or releasing hydrogen) and a replacement cell was used for background measurements while the first one was repaired.

The CNI experiment is very difficult for several reasons. It is a *singles* experiment, meaning that the recoil protons cannot be detected as they are not given enough energy to escape the target region. Also, the region of main interest at small scattering angles is close to the straight-through beam and overlaps the region populated by muons from pion decay. These two conditions make it impossible, in the usual CHAOS triggering system, to distinguish true elastic scatters from $\pi \rightarrow \mu\nu$ decays that occur in a substantial portion of the beam trajectory.

Another difficulty that must be addressed is that the cross section at forward angles is very steep. This means that the event sample would be strongly biased to the smallest scattering angles within the experimental acceptance, unless some form of selective pre-scaling is used. It also makes it necessary to have an accurate simulation of the angular resolution and solid angle in order to extract the differential cross section as a function of true scattering angle. In practice, the angular resolution varies with scattering angle as the vertical components of the incoming and outgoing momentum vectors play a more significant role at smaller scattering angles, and the vertical resolution of CHAOS is not as good as the horizontal resolution. Substantial progress on the simulation of the experimental conditions has been made over the past year.

To provide a check on the simulation and also as another basis for absolute normalization, the known μp cross section is measured simultaneously. The muon fraction of the M13 beam is quite small, as is the magnitude of the cross section compared with that for pions. This means that it is not desirable to do the same sort of scattering angle dependent pre-scaling that was proposed for beam pions.

Trigger

The above considerations led to several modifications of the CHAOS first and second level programmable triggers, both in hardware and software. The first layer of the π/μ stack was made the primary source of first level triggers for small scattering angles. Larger scattering angle data were also collected by allowing any one of the CHAOS fast trigger (CFT) blocks, covering the range of 30° to 240°, to also issue a first level trigger. In addition, a coincidence was made between signals from the in-beam counter and those from the capacitive probe (TCAP) near the production target. The timing was such that beam muons were identified to the first level trigger which was programmed to pre-scale events originating from the first three segments (5°—14°) of the first stack layer as long as they were not beam muons. Beam electrons were also identified by a similar coincidence and were not allowed to make triggers.

The traditional use of the CHAOS second level trigger has been to identify tracks with appropriate momentum and polarity that originate from the target region. This does not provide much rejection for CNI. Therefore, it was modified to identify and reject events where the outgoing track lines up with the incoming beam track. These events are typically straight-through beam pions that decay after passing through the inner chambers with the resulting muon missing the beam veto and striking one of the stack scintillators. The additional requirement that there be no extra hits in the inner chambers was incorporated so as not to veto backscatter π^+ events where the recoil proton follows a similar trajectory to a straight-through pion.

Even with these modifications, the bulk of the data collected were due to pion decays rather than elastic scattering. The first level trigger pre-scale factors (pions only) were approximately 3.8, 4 and 2 for the first three segments respectively. The comparatively smaller value of the first number was because a large fraction of the decay muons miss the first segment (striking the next two) and so it was not necessary to pre-scale it by as much as the steeply rising cross section might suggest. The second level trigger provided a rejection of about 50% and, in its new form, did not induce any extra sensitivity to the wire chamber efficiency. The resulting event rate was typically three to four times greater than previous CHAOS experiments with the live-time at a poor 55%. This shows the necessity of the pre-scaling.

Preliminary results

The CNI experiment received beam during the high intensity periods of 1999 in April–May and November–December. At each beam energy, a CNI measurement consisted of three parts: foreground, background and stack training. Each was performed at both polarities and, in some cases, at two target angles.

The stack training was performed first and consisted of a series of runs in which the beam was aimed at each of the eight segments of the first layer of the

π/μ stack. The whole procedure was applied at three beam momenta encompassing the momentum range of muons from pion decay. The purpose of these measurements is to train a neural network to provide particle identification based on all the information provided by the stack.

Foreground, background and training data were taken at both polarities with beam energies of 45 and 26 MeV. The CHAOS spectrometer and its associated trigger and data acquisition systems performed well throughout the year. Scatter plots of the intersection of the incoming beam with the outgoing scattered track are shown in Figs. 51 and 52. The former is from a run with a full LH_2 target and the latter is from a run with an empty target cell. The events in these figures are limited to scattering angles above 30°, which is greater than the angle of the muon cone, thus eliminating the large number of decay events. The 12.5 mm target cell is clearly seen in the foreground scatter plot. In both plots the support pillars and outer windows are also visible. Note that the target was not oriented perpendicular to the beam, but was rotated by 29°. The target pillars block particles scattered into them and so produce a *hole* in the measured angular distribution.

Events from the target region were then used to produce a scatter plot of momentum versus scattering angle. An example of these is shown in Fig. 53. The main band follows the kinematics of πp scattering and the hole centred at 120° is due to the target pillar. The large decay background is also clearly seen at forward angles. The forward angle region of these data is shown in Fig. 54. Although there is a substantial

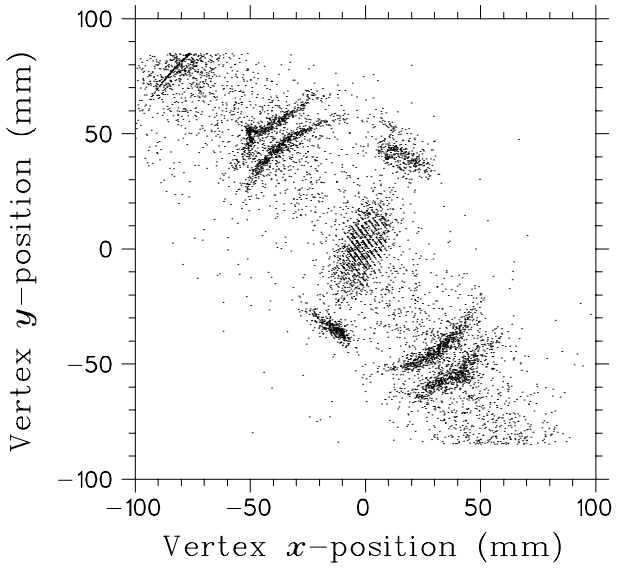

Fig. 51. The vertex position from π^+p scattering at 45 MeV. The 12.5 mm thick LH_2 target cell is clearly seen in the centre of the diagram. The regions on either side of the cell are the support pillars. The outer windows of the cryogenic target are also visible.

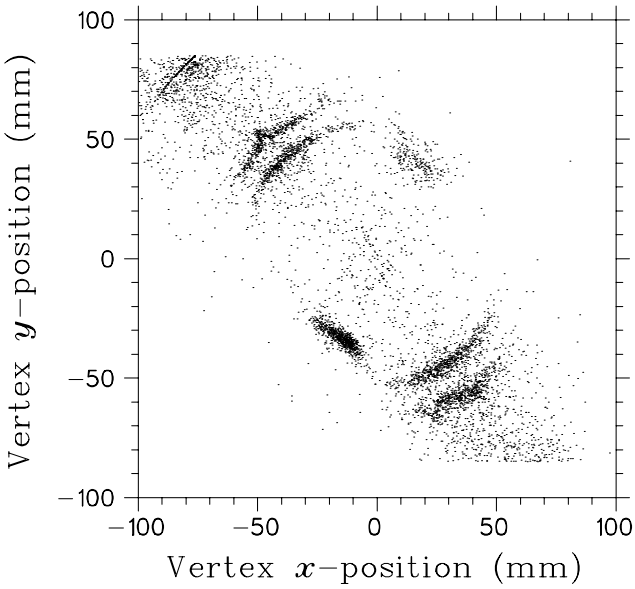

Fig. 52. The vertex position under the same conditions as those of Fig. 51 except that the target cell was empty.

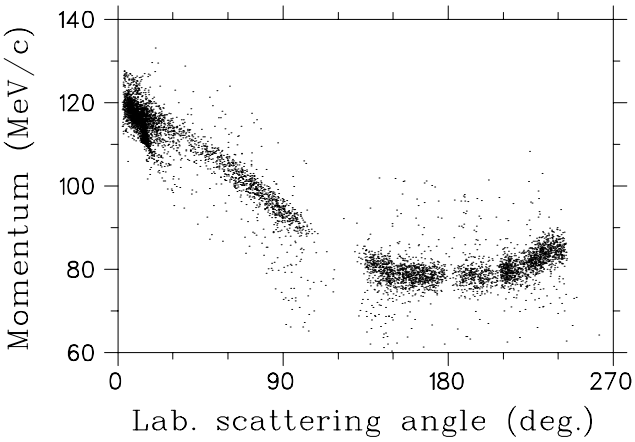

Fig. 53. Momentum vs. scattering angle from π^+p scattering at 45 MeV. The main band follows the expected kinematic behaviour and the hole at 120° is because one of the target pillars blocked particles scattered into that region.

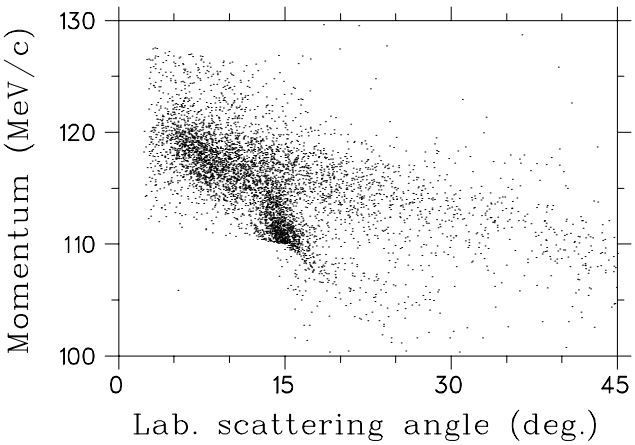

Fig. 54. Forward angle region of same data shown in Fig. 53. The bright band at ∼15° is due to $\pi \to \mu\nu$ events.

background that must be dealt with, it is clear that scattering angles as low as 5° have been successfully measured. At extreme forward angles, the incoming and outgoing tracks are nearly parallel so the vertex position obtained from their intersection has very poor resolution. To select events that scatter from the target region, a cut is made on the distance between the intersection points of the beam and scattered tracks with the central plane of the target.

At 45 MeV, data were also taken with a target angle of $-11°$ thus filling in the hole. At 26 MeV, only one orientation was used as it was desirable to maximize the statistics in the region of the S–P interference minimum. At this energy, the hole is in a region where the cross section is almost flat. Future measurements will be made at only one target orientation, chosen so that the hole does not overlap the interference minimum and is in a flat region of the cross section.

Conclusion

The target modifications meant that the CNI experiment finally had a stable operating target. This, combined with the excellent performance of the CHAOS spectrometer, led to a very productive year. Many experimental and analysis issues were resolved so that the planned running periods in 2000 are expected to be smooth and provide an extremely valuable data set. The computing power of the group has again been increased and improvements to the acquisition and analysis software may make it possible to perform a first pass skim of the data only hours after it is collected.

Experiment 781
Investigation of nuclear pion induced pion production

(M. Sevior, Melbourne)

The aim of this experiment was to measure the $\pi - \pi$ invariant distributions from the reactions $^{45}\mathrm{Sc}(\pi^+, \pi^+\pi^-)X$ and $^{45}\mathrm{Sc}(\pi^+, \pi^+\pi^+)X$ at the incident pion kinetic energies of 240, 260, 280, 300 and 320 MeV.

This is the continuation of TRIUMF experiment 653 which investigated the reactions:
$\pi^+ + d \rightarrow X\pi^+\pi^+$ and $\pi^+ + d \rightarrow X\pi^+\pi^-$
$\pi^+ + ^{12}\mathrm{C} \rightarrow X\pi^+\pi^+$ and $\pi^+ + ^{12}\mathrm{C} \rightarrow X\pi^+\pi^-$
$\pi^+ + ^{40}\mathrm{Ca} \rightarrow X\pi^+\pi^+$ and $\pi^+ + ^{40}\mathrm{Ca} \rightarrow X\pi^+\pi^-$
$\pi^+ + \mathrm{Pb} \rightarrow X\pi^+\pi^+$ and $\pi^+ + \mathrm{Pb} \rightarrow X\pi^+\pi^-$.

We found in that experiment that the invariant mass distributions for $\pi^+\pi^-$ for all nuclei differ substantially from the reaction on deuterium. We find substantially more yield (over a factor of 10) at the lowest invariant mass bins for reactions on nuclei compared to the reaction on deuterium. No such large deviation is observed for the $\pi^+\pi^+$ distributions on nuclei compared to deuterium.

There is yet to be a complete theoretical description of these results. However, the two most up-to-date theoretical investigations both agree that the best description of these data requires an anomalously large final state interaction between the outgoing $\pi^+\pi^-$ pairs. Perhaps the most exciting possibility is that the CHAOS data indicate the partial restoration of chiral symmetry within the nuclear medium. This possibility has been explored by Hatsuda, Kunihiro and Shimizu who have investigated how the isospin 0 $\pi - \pi$ interaction changes as a function of nuclear density in the presence of chiral restoration. They do indeed predict a substantial increase in the $\pi - \pi$ interaction very near threshold. This could manifest itself as a substantial final state interaction between the isospin 0 pions. However, Hatsuda *et al.* have not made a specific prediction for the nuclear $(\pi, 2\pi)$ reactions. If partial restoration of chiral symmetry is the explanation of the CHAOS data, it would be only the second example of obvious QCD or quark effects observed in nuclear physics. This approach has also been explored within a many-body framework by Aouissat *et al.* who agree that this approach can lead to a substantial increase in low energy strength of the isospin 0 $\pi - \pi$ interaction.

By measuring at a variety of bombarding energies Expt. 781 provides crucial extra information. The idea is that if the increase in yield is due to a final state interaction, the effect should be present at all bombarding energies. On the other hand, if the effect were due to some new in-medium production mechanism, the effect may change as a function of energy. The experiment was performed with the CHAOS spectrometer on the M11 channel at TRIUMF.

Further progress on the data analysis was made in 1999 and preliminary results of the measurement were presented at MENU 99 in Zuoz, Switzerland.

Our preliminary results are presented as the ratio of $\frac{(\pi^+\pi^-)}{(\pi^+\pi^+)}$ corrected for the different CHAOS acceptance for $(\pi^+\pi^-)$ compared with $(\pi^+\pi^+)$. These results are shown in Fig. 55.

As can be seen, the ratio of $\frac{(\pi^+\pi^-)}{(\pi^+\pi^+)}$ for ^{45}Sc is substantially different to that for the reactions on hydrogen at all bombarding energies. This is manifest as a substantial increase at low $(\pi^+\pi^-)$ invariant mass for scandium compared with hydrogen. In addition, our control reaction on CD_2 shows a very similar pattern to that for hydrogen, although the extra phase space available to the reaction on deuterium limits the range with which the data can be compared.

The preliminary CHAOS data confirm the previous result for ^{40}Ca at 280 MeV and show substantial differences to $\pi^- p \rightarrow \pi^+\pi^- n$ at all energies. Therefore

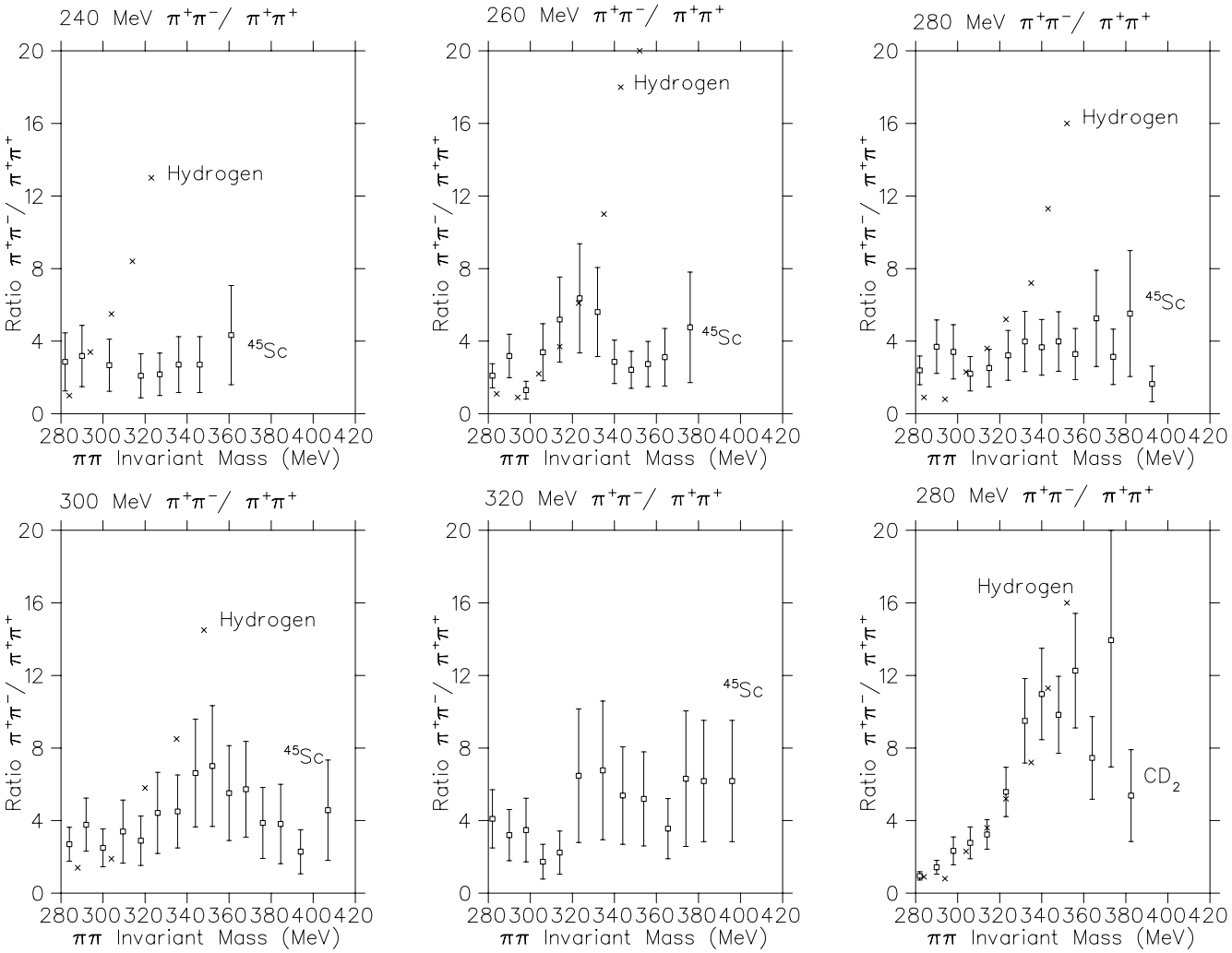

Fig. 55. Preliminary acceptance corrected ratios of $\frac{(\pi^+\pi^-)}{(\pi^+\pi^+)}$ at T_π = 240, 260, 280, 300 and 320 MeV as well as for CD_2 at T_π = 280 MeV. In each figure the crosses represent the ratio of the reaction on hydrogen and the squares are the results of the present measurement. In the case of 320 MeV, there was no previous hydrogen data available.

these data support the possibility that there is a substantial final state interaction in the isospin 0 channel of the $\pi - \pi$ interaction at nuclear densities. This is consistent with the hypothesis of Hatsuda *et al.* of the existence of partial restoration of chiral symmetry at nuclear densities.

We plan to complete the analysis of the these data in 2000 and aim to have submitted at least one paper for publication by the end of the year.

Experiment 785
Pion double charge exchange on ^{3}He with CHAOS
(R. Tacik, TRIUMF/Regina)

This experiment involved the measurement of both the inclusive $^3\mathrm{He}(\pi^-,\pi^+)$ and semi-exclusive $^3\mathrm{He}(\pi^-,\pi^+n)$ double charge exchange (DCX) reaction channels, at low incident pion energies. It is complementary to earlier Expts. 719 and 725 performed by the CHAOS collaboration.

One particularly novel feature of Expt. 785 was that it involved the simultaneous operation of CHAOS and an external time-of-flight neutron detector array. The hardware coincidence between the neutron array and CHAOS was made at the CHAOS second level trigger stage. Calibration data for the neutron array was obtained using charged particles from the incident and scattered beams, cosmic rays, and events from the $^3\mathrm{He}(\pi^-,dn)$ reaction, where the deuteron was detected in CHAOS. Experiment 785 employed the same basic Regina/TRIUMF liquid helium target as had been previously used for Expt. 725, but modified for L^{3}He instead of L^{4}He. The neutron array consisted of two layers. Each layer was composed of seven bars of plastic scintillator. Each bar had dimensions $15 \times 15 \times 105$

cm^3. The front face of the front layer was 350 cm from the centre of CHAOS. Three large plastic scintillator paddles positioned in front of the array were used to veto charged particles.

The general aim of Expt. 785 was to obtain high quality DCX data for ^{3}He with which to confront all models of the DCX process. No other measurements have been performed below $T_\pi = 120$ MeV. A more specific aim of Expt. 785 was to search for the existence of a narrow resonance in the πNN subsystem, called the d'. The effect of the d' has been proposed as the source of the otherwise unexplained behaviour of the total DCX cross sections near $T_\pi = 50$ MeV, as measured on virtually all heavier nuclear targets which have been studied. Use of the helium isotopes as targets provides the best potential for separating the influences of nuclear structure and the underlying DCX reaction mechanism.

Most of the Expt. 785 running time was spent on accumulating statistics in the neutron time-of-flight spectra for the semi-exclusive ^{3}He$(\pi^-, \pi^+ n)$ reaction. Measurements were taken at two angular settings of the neutron detector at an incident π^- energy of 75 MeV, and one angular setting at 65 MeV. Within the d' model, the reaction proceeds via the two-step process: $\pi^-\ ^3\mathrm{He} \rightarrow d'n \rightarrow (\pi^+ nn)n$. The detection of the π^+ in CHAOS serves as the signature of DCX. Because of the two-body intermediate state, the existence of the d' should manifest itself as a narrow peak in the neutron energy spectrum measured at a particular angle, above a combinatorial background arising from the detection of one of the neutrons from d' decay, rather than the one which recoiled against it in the intermediate state. Model calculations predict a smooth energy dependence for this background. The same holds true for neutrons produced via conventional mechanisms.

Preliminary results for the neutron TOF spectrum measured with $T_{\pi^-} = 75$ MeV at $\theta_n \simeq 11^\circ$ are given in Fig. 56. The data are represented by the solid histograms and are repeated three times to facilitate comparison with model predictions. The model predictions are represented by the dashed histograms, and the curves shown are 'best fit' ones. The upper plot in Fig. 56 shows the comparison with the predictions of a conventional sequential single charge exchange (SSCX) model. The comparison with the d' model, which predicts a sharp peak above a smooth background, is shown in the middle plot. The lower plot shows the comparison with four-body phase space, which assumes that all three nucleons in ^{3}He participate in the DCX reaction. Clearly, the data do not favour the d' model. The best description of the data is provided by a combination of the four-body phase space and SSCX curves.

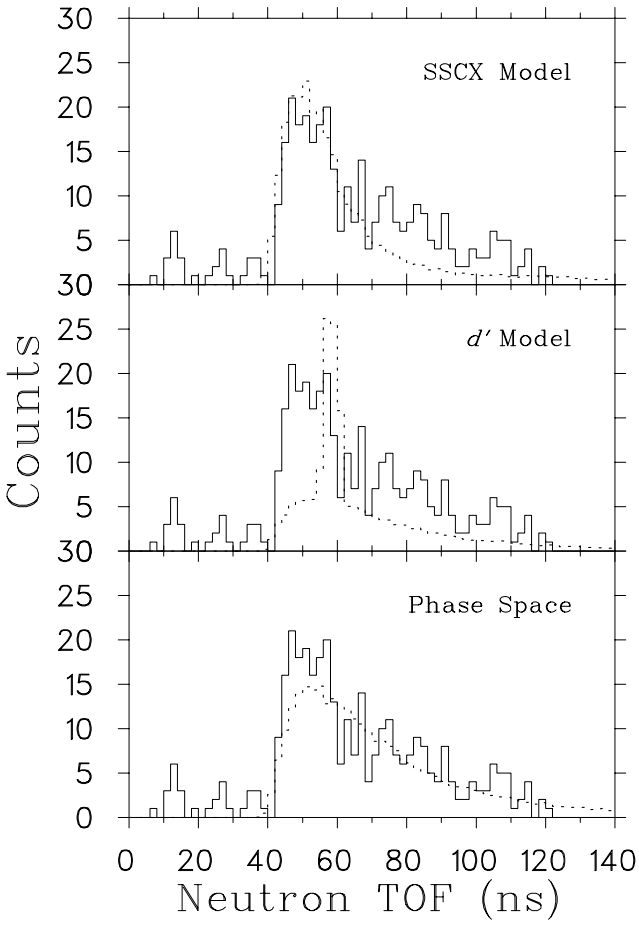

Fig. 56. Neutron time-of-flight distribution measured in Expt. 785. The solid histogram represents the data, the dashed histograms represent the predictions of various model calculations.

A relatively smaller part of the Expt. 785 running time was spent on the inclusive ^{3}He(π^-, π^+) reaction. Data were taken at several incident pion energies between 65 and 120 MeV. Total cross sections were determined by extrapolating measured $d^2\sigma/d\Omega dp$ differential distributions. The analysis of this part of the experiment formed part of the Ph.D. thesis project of Mr. J. Graeter from the University of Tübingen. More details can be found in an article by J. Graeter *et al.*, which will appear in Phys. Lett. B.

Results are shown in Fig. 57. The solid curve in this figure represents the results of an on-shell Monte Carlo model of the conventional SSCX mechanism. The dashed curve represents the original prediction based on the d' model [Clement *et al.*, Phys. Lett. **B337**, 43 (1994)]. The data clearly lie far below the prediction. However, it has been pointed out that the original prediction ignored the possibility of 'collision damping'. That is, rather than decay, $d' \rightarrow NN\pi$, the d', once formed, may disappear via the $d'N \rightarrow NNN$ reaction. Accounting for 'collision damping' reduces the prediction of the d' contribution to the total DCX

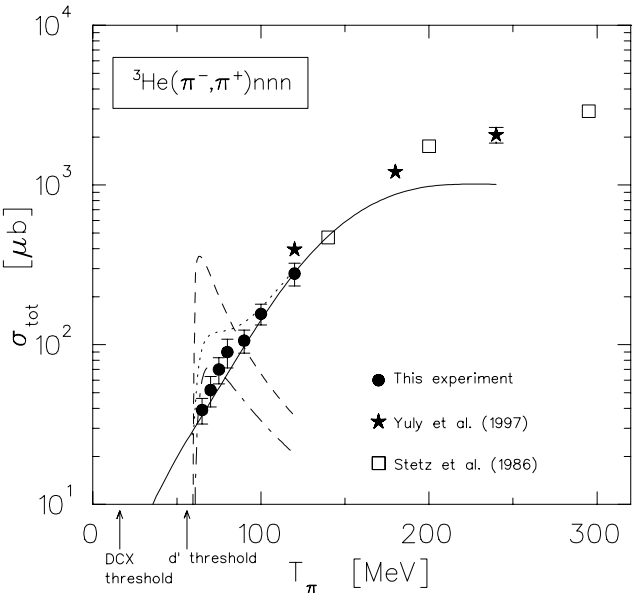

Fig. 57. Total cross section for the ^{3}He(π^-,π^+) reaction. See text for details.

cross section considerably. The dash-dotted curve in Fig. 57 shows the results of the d' calculation including the estimated effect of this process. The dotted line in Fig. 57 is the incoherent sum of the calculations represented by the solid and dash-dotted curves.

Naturally, the 'collision damping' effect should also affect the predictions for the DCX on ^{4}He, which were measured in Expt. 725. The new predictions are shown in Fig. 58. Here, the solid curve represents the results of an on-shell Monte Carlo model of the conventional SSCX mechanism, the dashed curve the d' calculation using a Gaussian ^{4}He wave function without 'collision damping', and the dot-dashed curve the

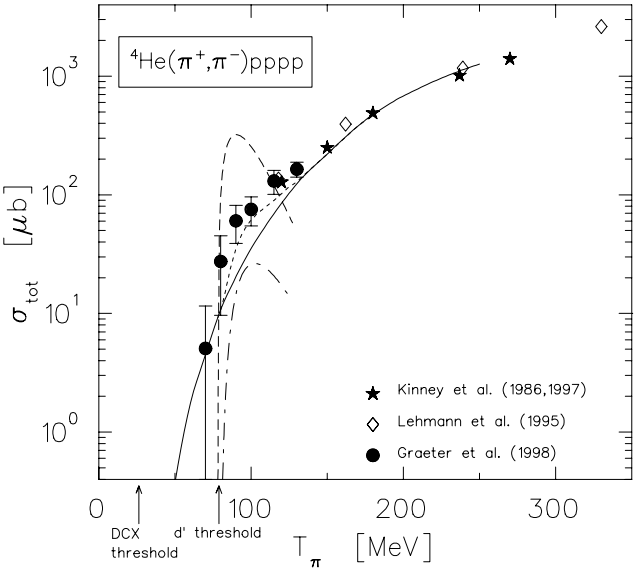

Fig. 58. Total cross section for the ^{4}He(π^+,π^-) reaction. See text for details.

d' calculation for the Gaussian ^{4}He wave function with 'collision damping'. The dotted line is the incoherent sum of the conventional calculation and the d' calculation with 'collision damping'.

Experiment 823
Pure Fermi decay in medium mass nuclei
(G.C. Ball, TRIUMF; D.M. Moltz, LBL)

Precise measurements of the intensities for superallowed Fermi $0^+ \rightarrow 0^+$ β-decays have provided a demanding test of the CVC hypothesis at the level of 3×10^{-4} and also led to a result in disagreement with unitarity (at the 98% confidence level) for the CKM matrix [Towner and Hardy, WEIN'98]. Since this would have profound implications for the minimal standard model it is essential to address possible trivial explanations for this apparent non-unitarity, such as uncertainties in the theoretical isospin symmetry-breaking correction. Uncertainties in the calculated Coulomb corrections can be studied by extending the precision β-decay measurements to heavier (A $\geq$ 62, $T_z = 0$) odd-odd nuclei where these corrections are predicted to be much larger [Ormand and Brown, Phys. Rev. **C52**, 2455 (1995)]. The primary goal of the Expt. 823 program is to measure the half-lives and branching ratios for the superallowed β-decay of these radioactive nuclei produced at ISAC.

Precision lifetime measurements for ^{37}K and ^{38m}K

In April and May beam time was obtained to measure the half-lives of the first beams available from ISAC, namely ^{38m}K and ^{37}K. The measurement on ^{38m}K, one of the nine well-known superallowed β transitions, provides an important test of the experimental apparatus. In addition, a more precise measurement of the half-life for ^{37}K ($t_{1/2} = 1226 \pm 7$ ms) is required for the high priority TRINAT Expt. 715.

The experiments were carried out at ISAC using the techniques described in detail in the 1998 Annual Report. Approximately 60 runs, each consisting of 100–300 cycles with a total of 4–16 $\times 10^6$ events per run, were obtained for the beta decay of ^{37}K. Systematic errors introduced by the measurement techniques were determined by making the measurements under a variety of experimental conditions. A 30% efficient HPGe detector located just outside the 4π counter was used to monitor the sample purity.

During the ^{37}K run, measurements were also made to optimize the ratio for the yield of ^{38m}K to the long-lived (7.6 m) isobaric contaminant ^{38}K. By collecting a sample for $\sim$0.3 s it was only possible to reduce the initial count rate for ^{38}K to $\sim$14% of the initial count rate for ^{38m}K. Next, the proton beam was turned off and measurements were made of the release time of the

^{38}K from the target. The yield was found to come from a fast (∼30 s) component and a slow (∼6 m) component. When the proton beam was left off for ∼0.5 h the ratio of the yields for ^{38m}K/^{38}K was increased to 40:1 in the first sample obtained after the beam was turned on. These results showed that a measurement of the half-life for ^{38m}K with the required precision was possible if the proton beam was pulsed with a duty cycle of 10%. This was done for two shifts during the second running period from May 8–13. Ten runs, each consisting of ∼4 million events, were obtained while pulsing the proton beam on for 3 seconds every 30 seconds. The ratio of the yields for ^{38m}K/^{38}K was ∼25:1. Ten runs of unpulsed data were also obtained.

The data analysis was carried out both at TRIUMF and at Texas A&M using the methods described elsewhere [Koslowsky *et al.*, Nucl. Instrum. Methods **A401**, 289 (1997)]. After eliminating low statistics and noisy samples, the remaining data were analyzed by two methods: 1) simultaneously fitting all data samples with a single half-life parameter and variable intensities and backgrounds, and 2) by summing the dead-time-corrected data for all samples and then fitting with a single half-life, intensity and background. Both methods were found to give identical results.

For ^{37}K the statistical error in the measured half-life for each run varied from ∼0.3–0.8 ms; a typical decay curve is shown in Fig. 59. This resulted in a statistical error in the weighted average of all measurements of ∼0.08 ms. The additional error resulting from the uncertainty in the measurement of the fixed dead times was ∼0.07 ms. A determination of the systematic errors is not yet completed but a preliminary estimate is <0.2 ms. Possible impurites in the ^{37}K samples were estimated from the gamma-ray spectra taken during the first 3 seconds of each cycle. For ^{37}Ca a limit of ∼0.1% was obtained. Since ^{37}Ca has a half-life of 175 ms its effect on the measured half-life of ^{37}K can be estimated by fitting the data starting one or two half-lives from $t = 0$; no observable difference was observed within errors. From these data the preliminary value for the lifetime for ^{37}K is 1235.3 ± 0.3 ms.

For ^{38m}K the statistical error in the fitted half-life for each run was ∼0.8–1.1 ms for both the pulsed and the unpulsed data sets (Fig. 60). This resulted in a statistical error in the weighted average from each data set of ∼0.3 ms. From a preliminary analysis of these data we obtain values of 924.8 ± 0.3 ms and 925.1 ± 0.3 ms for the pulsed and unpulsed data sets, respectively. The errors quoted are statistical only and estimates of the systematic errors are in progress. The present values are in agreement with the weighted average, 923.98±0.64 ms, of previous measurements [Koslowsky *et al.*, Nucl. Phys. **A405**, 29 (1983)].

Measurements of polarization asymmetries in the β-decay of ^{37}K

Precision measurements that would test the standard model can be made by measuring polarization

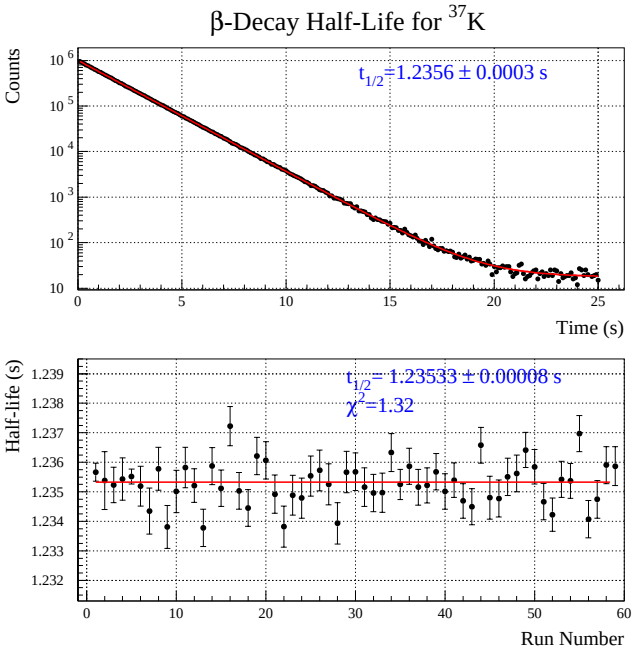

Fig. 59. β-decay half-life for ^{37}K. The upper plot shows the fit to the data of one run. Below are shown the results from all runs and the (preliminary) mean value obtained.

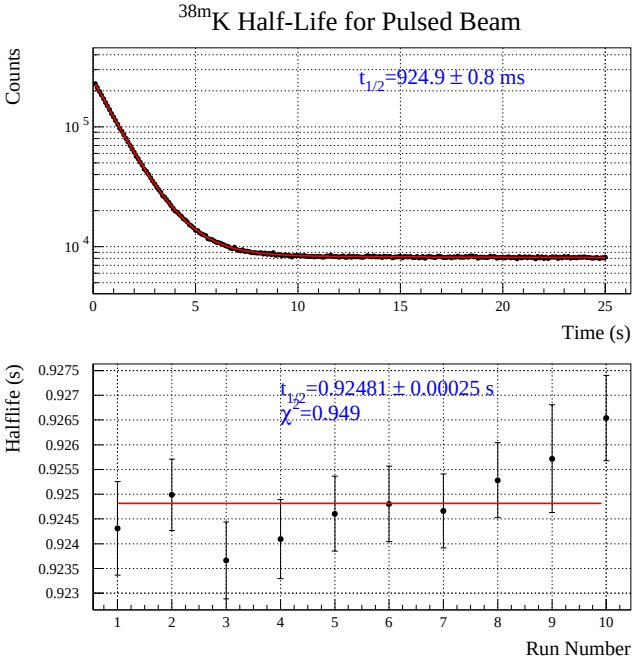

Fig. 60. β-decay half-life for ^{38m}K obtained with the pulsed proton beam on the production target. The upper plot shows the fit to the data of one run. Below are shown the results from all runs and the (preliminary) mean value obtained.

asymmetries in the β-decay of non-zero spin nuclei. The decay probability dW is given by [Häusser, Nucl. Phys. **A585**, 133c (1995)]:

$$dW = dW_0\xi(1 + a\beta\cos\theta_{e\nu} + AP\beta\cos\theta_{ej} + BP\cos\theta_{j\nu} + cc_P\beta[\cos\theta_{j\nu}\cos\theta_{ej} - \frac{1}{3}\cos\theta_{e\nu}]),$$

where $dW_0\xi$ is the rate in the absence of correlations, β is p/E with p the electron momentum and E the electron energy, c_P is the polarization parameter $[-J(J+1)+3P^2J^2]/J(2J-1)$ which varies strongly with the nuclear polarization P, and $\vec{j}$ is a unit vector in the direction of the vector polarization $< J >$. The β–ν correlation parameter a, the β and ν asymmetry parameters A and B, respectively, and the polarization coefficient c depend on the nuclear spin, J, and the ratio of the matrix elements $\lambda = G_A M_{GT}/G_V M_F$.

Preliminary values of the non-zero correlation parameters in ^{37}K can be calculated using the recently determined branching ratio, $97.89 \pm 0.11\%$ [Hagberg *et al.*, Phys. Rev. **C56**, 135 (1997)], and the β-decay half-life measured at ISAC. The standard model predictions for a, A, B and c are shown in Table VIII. The errors in the correlation parameters were calculated assuming an error of 1 and 0.1 ms in the β-decay half-life. In the present experiment it should be possible to reduce this error to <0.5 ms, therefore the uncertainties in the correlation parameters are now dominated by the error in the branching ratio.

Table VIII. Observables in ^{37}K decay[a].

Observable	a	A	B	c
value	0.6683	–0.5702	–0.7692	0.1990
error[b]	0.0016	0.0006	0.0015	0.0009
	(0.0013)	(0.0005)	(0.0013)	(0.0008)

[a] Calculated within the standard model with $\lambda = -0.5754 \pm 0.0016$ corresponding to a ^{37}K half-life of 1253.3 ± 1.0 ms.

[b] Errors in parentheses were calculated for an error in the ^{37}K half-life of ± 0.1 ms.

First results for the lifetime of ^{74}Rb

In July–August a Nb foil target was used at ISAC to produce ^{74}Rb. The yield obtained was ~440 ions μA^{-1}s^{-1} of protons on target, comparable to the yields previously observed at ISOLDE. The target was bombarded for several weeks at a proton beam current of 10 μA with no noticeable decrease in yield (i.e., 5–10 times the previous ISOLDE yield). The only previous measurement of the half-life (64.9 ± 0.5 ms) of ^{74}Rb was carried out by J.M. D'Auria *et al.* [Phys. Lett. **66B**, 233 (1977)]. During the run at ISAC we obtained over 100 times more data which should allow us to reduce the error in the lifetime by more than a factor of ten.

After the lifetime apparatus was moved to a permanent location in June, several changes were made to optimize the experimental set-up for the ^{74}Rb lifetime measurements. The distance from the differential slit box to the gas counter was shortened and the speed of the tape transport system was doubled to 5 m s^{-1}. With these changes it was possible to move the sample to the 4π counter and begin counting within 100 ms. A plastic scintillator was positioned inside the collection chamber directly behind the tape. This was used to tune the radioactive beam and to monitor the buildup of activity on the tape sample by sample. During this run the LEBT transport efficiency from the mass separator to the collection chamber was only ~50%, and the average number of counts obtained was ~80 per sample. With dwell times of ~6 ms per channel the total cycle time was ~3 s. Twenty-four runs each consisting of $\sim 4 \times 10^5$ events were obtained. The data from one run are shown in Fig. 61. A small (~1%) long-lived background component was observed in the decay curves which was identified in the gamma-ray spectra as ^{74}Ga ($t_{1/2} = 8.12$ m). The analysis of these data is in progress. A preliminary result obtained from the analysis of 13 runs (see Fig. 61) gives a weighted average of 64.75 ± 0.04 ms, in good agreement with the previous measurement. The error quoted is the statistical error only. Additional running time was obtained

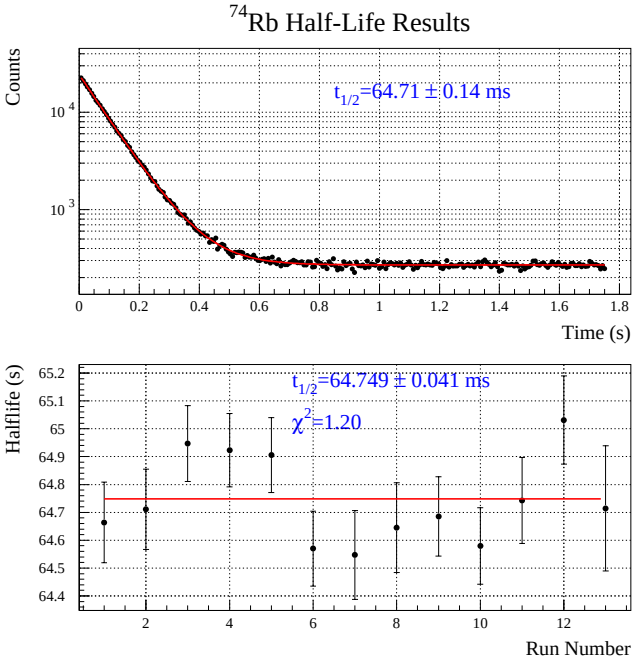

Fig. 61. β-decay half-life for ^{74}Rb. The upper plot shows the fit to the data of one run. Below are shown the results from several runs and the (preliminary) mean value obtained.

in November. If no unexpected systematic errors are present in these data then the required precision of 0.05% should be obtainable.

Since the Q-value for the β-decay of ^{74}Rb is large ($\sim$10 MeV), several potential weak branches to excited $(0,1)^+$ states in ^{74}Kr, which subsequently gamma decay, may need to be determined. These demanding measurements (due to the short half-life and limited beam intensity) will be the primary objective for Expt. 823 in the coming year.

Experiment 838
Two-photon capture mode of pionic hydrogen
(P. Żołnierczuk, T. Gorringe, Kentucky)

Pionic hydrogen is formed when negative pions are stopped in liquid hydrogen. The pionic hydrogen atom subsequently disintegrates via one of several capture modes. The dominant capture modes $\pi^- p \to \pi^o n$, $\pi^- p \to \gamma n$, and $\pi^- p \to e^+ e^- n$ have well determined branching ratios. However, until this experiment, the much rarer capture mode $\pi^- p \to \gamma\gamma n$ had not been measured.

For capture from the $1S$ atomic state, the predicted mechanism for the $\pi^- p \to \gamma\gamma n$ reaction is the annihilation of the real π^- and a virtual π^+ into a photon-pair (i.e. $\pi^-\pi^+ \to \gamma\gamma$). Crossing symmetry relates the $\pi^-\pi^+ \to \gamma\gamma$ annihilation diagram to $\gamma\pi \to \gamma\pi$ Compton scattering, and offers potential sensitivity to the pion's electric polarizability. The predicted branching ratio is 0.51×10^{-5} [Beder, Nucl. Phys. **B156**, 491 (1979)].

We have completed a test run in June, 1997 and two production runs in December, 1998 and April/May, 1999. In the June '97 test run we tested the two-photon trigger and measured the two-photon acceptance. In the December '98 and April/May '99 production runs we collected approximately one thousand $\pi^- p \to \gamma\gamma n$ events. A sample two-gamma event is shown in Fig. 62.

Our sample of the two-gamma events is almost background free in the opening angle region $\theta \leq 100^\circ$ (or $\cos\theta \geq -0.2$). A preliminary opening angle distribution of the two-photon events is presented in Fig. 63. The two main sources of backgrounds – $\pi^o \to \gamma\gamma$ decay and accidental events – are small. We plan to present our preliminary results at the MESON'2000 conference in Poland and CIPANP'2000 in Canada.

In parallel, the TRIUMF Theory Group is calculating the $\pi^- p \to \gamma\gamma n$ process in the framework of χPT.

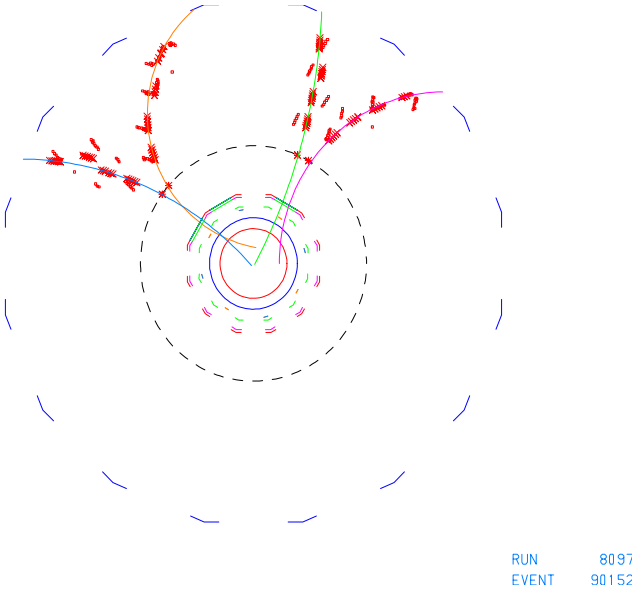

Fig. 62. A sample small opening angle two-photon event.

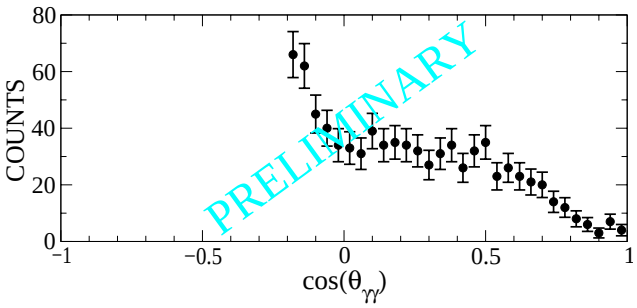

Fig. 63. Opening angle distribution for the two-photon events following pion stops in hydrogen.

Experiment 862
Polarization observables in the $\vec{p}(\pi^\pm, \pi^+\pi^\pm)$ reactions: a test of chiral perturbation theory
(R. Tacik, TRIUMF/Regina)

This experiment was approved with high priority by the TRIUMF EEC in May.

The experiment consists of measurements of asymmetries in the two reactions $\pi^+\vec{p} \to \pi^+\pi^+ n$ and $\pi^-\vec{p} \to \pi^+\pi^- n$ at several incident pion energies. The broad goal of the experiment is to test the predictions of χPT, which has emerged as a precision tool in low energy hadron physics. Pion induced pion production off nucleons has recently been studied in the framework of heavy baryon χPT to chiral order three by two groups [Zhang *et al.*, nucl-th/9806063; Fettes *et al.*, hep-ph/9907276]. Although the published calculations did not include predictions for polarization observables, we have been assured by both groups that their work can be extended to include polarization effects.

Generally, we expect to learn whether polarization observables can be described consistently in χPT. Up until recently, the existing database for the pion production reactions consisted mostly of total cross section measurements. CHAOS Expt. 624 provided the first extensive measurements of differential distributions. Experiment 862 will provide the world's first measurement of polarization observables.

More specifically, one of the original motivations for the investigation of the pion induced pion production reactions was the extraction of fundamental pion-pion scattering parameters. Fettes, Bernard, and Meissner point out that "it is conceivable that some polarization observables will be more sensitive to the pion-pion interaction than the unpolarized observables" which have been studied to date. These authors also intimate that polarization observables would give a handle on the question of whether the standard or so-called generalized scenario of spontaneous symmetry breaking is more appropriate, i.e. a large or small scalar quark condensate.

Another specific issue is the determination of the values of the low energy constants (LECs) which appear in χPT. At third order, there are six new LECs. Attempts have been made to determine the values of these LECs by fitting χPT results to the existing observables, including especially the CHAOS differential distributions from Expt. 624. The Meissner group found that two pairs of LECs are almost perfectly anticorrelated, so that only four can be determined. Polarization observables will help to resolve this.

Apart from the χPT calculations, there exist several model calculations for the pion production reactions in which tree level graphs are supplemented by explicit Δ and N^* contributions. Since polarization effects stem from the interference of real and imaginary parts of certain invariant amplitudes, comparison with polarization data will be able to differentiate between different theoretical approaches.

Experimentally, Expt. 862 is quite challenging since it requires the measurement of small cross sections and the use of a polarized target. The CHAOS collaboration has already demonstrated its ability to handle such challenges in Expt. 624 and Expt. 560. The latter experiment made use of a polarized proton target. One new feature of Expt. 862 will be background arising from pion induced pion production on nuclei present in the target material. This will be eliminated by explicit measurement and subtraction.

We plan to start running Expt. 862 after the completion of data-taking for Expt. 778, and the relocation of the CHAOS detector from the M13 channel to the M11 channel at TRIUMF.